Gfra1 Underexpression Causes Hirschsprung's Disease and Associated Enterocolitis in Mice

Porokuokka, L. Lauriina

2019

Porokuokka , L L , Virtanen , H T , Linden , J , Sidorova , Y , Danilova , T , Lindahl , M , Saarma , M & Andressoo , J-O 2019 , ' Gfra1 Underexpression Causes Hirschsprung's Disease and Associated Enterocolitis in Mice ' , Cellular and Molecular Gastroenterology and Hepatology , vol. 7 , no. 3 , pp. 655-678 . https://doi.org/10.1016/j.jcmgh.2018.12.007

http://hdl.handle.net/10138/301616
https://doi.org/10.1016/j.jcmgh.2018.12.007

cmgh
CELLULAR AND MOLECULAR GASTROENTEROLOGY AND HEPATOLOGY

ORIGINAL RESEARCH

Gfra1 Underexpression Causes Hirschsprung's Disease and Associated Enterocolitis in Mice

L. Lauriina Porokuokka,[1] Heikki T. Virtanen,[1] Jere Lindén,[2] Yulia Sidorova,[1] Tatiana Danilova,[1] Maria Lindahl,[1] Mart Saarma,[1,§] and Jaan-Olle Andressoo[1,§]

[1]Institute of Biotechnology, and [2]Department of Veterinary Biosciences, Faculty of Veterinary Medicine, University of Helsinki, Helsinki, Finland

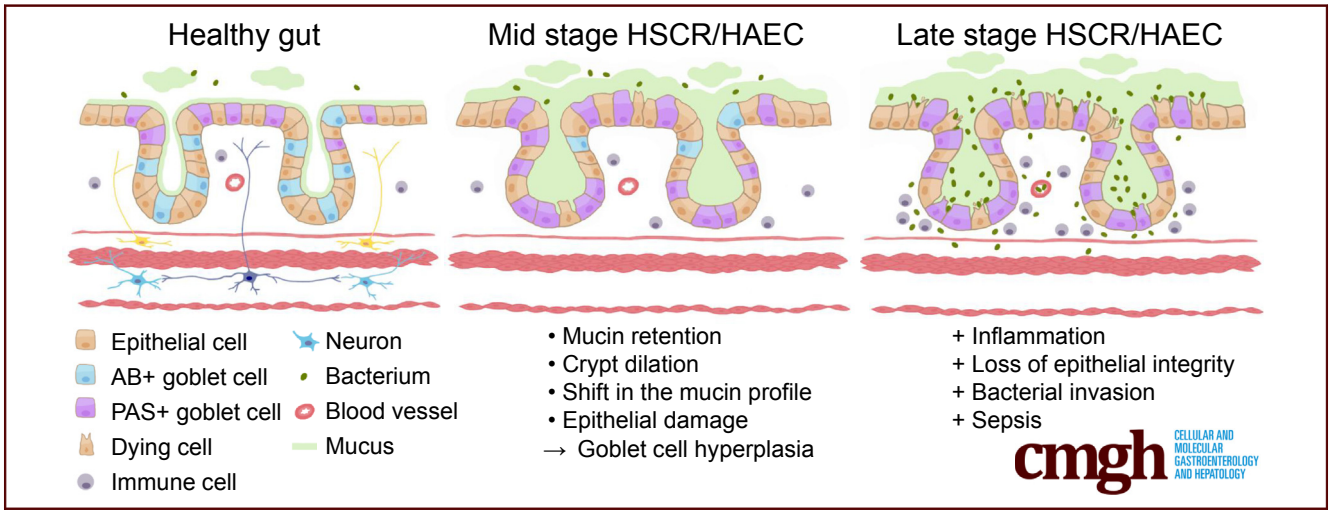

SUMMARY

A 70% to 80% underexpression of glial cell line–derived neurotrophic factor family receptor alpha-1 results in Hirschsprung's disease and an associated enterocolitis phenotype in a new mouse model. Enterocolitis proceeds from goblet cell dysplasia, with mucin abnormalities, to epithelial damage. Reduced expression of glial cell line–derived neurotrophic factor family receptor a1 may contribute to Hirschsprung disease susceptibility.

BACKGROUND & AIMS: RET, the receptor for the glial cell line–derived neurotrophic factor (GDNF) family ligands, is the most frequently mutated gene in congenital aganglionic megacolon or Hirschsprung's disease (HSCR). The leading cause of mortality in HSCR is HSCR-associated enterocolitis (HAEC), which is characterized by altered mucin composition, mucin retention, bacterial adhesion to enterocytes, and epithelial damage, although the order of these events is obscure. In mice, loss of GDNF signaling leads to a severely underdeveloped enteric nervous system and neonatally fatal kidney agenesis, thereby precluding the use of these mice for modeling postnatal HSCR and HAEC. Our aim was to generate a postnatally viable mouse model for HSCR/HAEC and analyze HAEC etiology.

METHODS: GDNF family receptor alpha-1 (GFRa1) hypomorphic mice were generated by placing a selectable marker gene in the sixth intron of the *Gfra1* locus using gene targeting in mouse embryonic stem cells.

RESULTS: We report that 70%–80% reduction in GDNF co-receptor GFRa1 expression levels in mice results in HSCR and HAEC, leading to death within the first 25 postnatal days. These mice mirror the disease progression and histopathologic findings in children with untreated HSCR/HAEC.

CONCLUSIONS: In GFRa1 hypomorphic mice, HAEC proceeds from goblet cell dysplasia, with abnormal mucin production and retention, to epithelial damage. Microbial enterocyte adherence and tissue invasion are late events and therefore unlikely to be the primary cause of HAEC. These results suggest that goblet cells may be a potential target for preventative treatment and that reduced expression of GFRa1 may contribute to HSCR susceptibility. *(Cell Mol Gastroenterol Hepatol 2019;7:655–678; https://doi.org/10.1016/j.jcmgh.2018.12.007)*

Keywords: Aganglionosis; Megacolon; Transgenic Mouse Model.

Hirschsprung's disease (HSCR, also known as congenital intestinal aganglionosis) is a congenital malformation characterized by a lack of enteric ganglia in the distal part of the gut leading to constipation, gut

distention, and associated failure to thrive. The underlying pathogenic etiology is widely accepted to be based on defects in craniocaudal migration, proliferation, differentiation, and survival of neuroblasts that originate from the neural crest in the early stage of pregnancy.[1,2] The prevalence of HSCR is 1 in 5000 live births, and the disease generally is subdivided into short-segment and long-segment types based on the point at which histologically characterized aganglionosis begins. Currently, HSCR routinely is treated by surgical removal of the aganglionic gut segment. The most life-threatening HSCR-associated complication is HSCR-associated enterocolitis (HAEC), which can occur preoperatively and/or postoperatively.[3] HAEC develops in approximately 30% of patients with short-segment and 50% of patients with long-segment HSRC.[4,5] The incidence of HAEC suggests either a multigenic and/or environmental contribution,[4,6] but the pathogenesis of HAEC remains poorly understood. Mucosal barrier dysfunction as a predisposing factor is one of the several proposed drivers for HAEC.[4–6] HAEC is clinically characterized by fever, abdominal distention, diarrhea, and sepsis. Histopathologic features in the colon include crypt dilatation, mucin retention, enterocyte adherence of bacteria, a shift from acidic toward neutral mucin production, epithelial damage, leukocyte infiltration, ulceration, and, in the terminal stages, transmural necrosis and perforation.[4–7] However, at least in part owing to a lack of suitable animal models, the order in which these HAEC-associated clinical features develop is currently poorly understood, which has hampered advances in the treatment and prevention of HAEC.

The most common genetic cause of HSCR is the presence of inactivating mutations in the receptor tyrosine kinase rearranged during transfection (RET), the signaling receptor for glial cell line–derived neurotrophic factor (GDNF); approximately 50% of cases are familial, and 15%–35% are sporadic cases.[2,8–11] In addition, at least 13 other HSCR susceptibility genes have been identified, including *GDNF*, *NRTN*, *EDNRB*, *EDN3*, *ECE1*, *SOX10*, *PHOX2B*, *KIF1BP*, *ZEB2*, *TCF4*, and *TTF1*; together, mutations in these genes account for approximately 20% of all HSCR cases.[2,9,12,13] HSCR penetrance also is known to be influenced by gene expression levels because copy number variants of *MAPK10*, *ZFHX1B*, and *SOX2* loci were associated with HSCR in a pilot study on 67 candidate genes.[12] Currently, the underlying genetic cause is unknown for approximately half of all sporadic cases of HSCR.[2,9]

RET is activated upon binding with a complex comprising GDNF and GDNF family receptor alpha-1 (GFRa1), a glycosylphosphatidylinositol-anchored protein.[14] Studies using transgenic mice have shed light on how GDNF signaling regulates the development of the enteric nervous system (ENS). In the developing mouse gut, ENS progenitor cells called enteric neural crest–derived cells (ENCCs) enter the foregut on embryonic day 9–9.5 (E9-E9.5). ENCCs migrate rostrocaudally along the gut toward a GDNF source, reach the proximal colon at E12, and colon colonization is complete by E14.5.[15,16] In addition to regulating ENCC migration, GDNF signaling also controls the proliferation, differentiation, and survival of ENCCs.[17–19] Mice that lack expression of genes encoding GDNF, GFRa1, or RET have a common phenotype that includes kidney agenesis and a lack of enteric ganglia distal to the stomach.[20–22] However, heterozygous *Gdnf*, *Gfra1*, or *Ret* null-allele mice with a reduced gene dose have a relatively mild reduction in enteric neuron numbers and do not develop the clinical features of childhood HSCR or HAEC.[23] Mouse studies using knock-in or timed conditional deletion alleles for *Gfra1* or *Ret* support the importance of GFRa1/RET signaling in ENS development and survival through postnatal day 1 (P1).[18,24,25] However, animal models with defective GDNF/GFRa1/RET signaling that phenocopy postnatal HSCR and/or HAEC are currently not available.

Mutations in the *RET* gene are the most common genetic cause of HSCR, however, causative mutations in *GFRa1* have not been found. Here, we report the generation of GFRa1 hypomorphic mice with reduced expression of *Gfra1* at the endogenous locus. These mice were generated by inserting a selectable marker gene within intron 6 of the *Gfra1* gene. Homozygous GFRa1 hypomorphic ($Gfra1^{hypo/hypo}$) mice have a 70%–80% reduction in *Gfra1* expression in the developing gut and kidney. Although the kidneys develop normally, $Gfra1^{hypo/hypo}$ mice have congenital features reminiscent of childhood long-segment HSCR, with early postnatal onset of symptoms and accompanying progressive HAEC; these mice generally die at P7–P25. Our further analysis also suggests a possible explanation why reduced gene expression in heterozygous *Gdnf*, *Gfra1*, and *Ret* null-allele mice does not result in HSCR, whereas a more severe reduction in *Gfra1* expression in $Gfra1^{hypo/hypo}$ mice does lead to HSCR. In addition, our analysis of $Gfra1^{hypo/hypo}$ mice has enabled us to better define the sequence of events in the pathogenesis of HAEC. Specifically, our results allow us to exclude bacterial enterocyte adherence as the primary cause of HAEC in our model, and suggest that goblet cell dysplasia is an early, ubiquitous event that precedes the epithelial changes, including crypt dilatation, mucin retention, and epithelial damage. Together, these findings suggest that goblet cells

§Authors share co-senior authorship.

Abbreviations used in this paper: AB, Alcian Blue; cDNA, complementary DNA; E, embryonic day; ELISA, enzyme-linked immunosorbent assay; ENCC, enteric neural crest-derived cell; ENS, enteric nervous system; GDNF, glial cell line–derived neurotrophic factor; GFRa1, glial cell line–derived neurotrophic factor family receptor alpha-1; GI, gastrointestinal; HAEC, Hirschsprung's disease–associated enterocolitis; HPF, high-power field; HSCR, Hirschsprung's disease; IL, interleukin; KO, knockout; LMMP, longitudinal muscle/myenteric plexus preparation; mRNA, messenger RNA; NADPH, reduced nicotinamide adenine dinucleotide phosphate; P, postnatal day; PAS, periodic acid–Schiff; PBS, phosphate-buffered saline; PCR, polymerase chain reaction; qPCR, quantitative polymerase chain reaction; RET, rearranged during transfection; TBS, Tris-buffered saline; TNF, tumor necrosis factor; WT, wild type.

Most current article

2352-345X
https://doi.org/10.1016/j.jcmgh.2018.12.007

could be a candidate target for developing preventative therapies for HAEC and that reduced expression of GFRa1 may represent a novel susceptibility trait for HSCR.

Results

Generation and Primary Characterization of Gfra1$^{hypo/hypo}$ *Mice*

Insertion of a marker gene into an intron of a target gene often interferes with expression of the target, yielding a hypomorphic allele.[26–30] We inserted a puΔtk cassette[31] into intron 6 of the *Gfra1* gene (Figure 1*A–C*) and analyzed the phenotype of homozygous (*Gfra1*$^{pu\Delta tk/pu\Delta tk}$) mice generated by crossing 2 heterozygous animals. Compared with their expected Mendelian inheritance, homozygous mice were under-represented by approximately 3- to 4-fold at the time of weaning (P18–P25); moreover, homozygous mice developed severe abdominal swelling, failed to thrive, showed increasing inactivity, and other signs of discomfort. Of the 8 homozygous mice that were monitored beginning at P15, none survived beyond P27; because of ethical considerations, we did not proceed with subsequent survival studies. During further experiments, animals that showed obvious signs of discomfort, including abdominal swelling, cachexia, and inactivity, were euthanized. One or more of those signs usually became evident by P4, with gradual progression until the end stage/euthanasia, usually between P7 and P25. Necropsy performed at P18–P25 showed marked caudal gut distention (Figure 1*D*) starting between the distal ileum and the midcolon. Four of 8 homozygous animals analyzed at P18–P25 had acute erythema/hyperemia in the gastrointestinal (GI) tract, indicative of acute inflammation (Figure 1*D*, right panel). Upon further inspection, narrowed, contracted gut that was distal to the distention was less flexible and stiff, a feature commonly reported for aganglionic gut segments in HSCR patients.

Analysis of Gfra1, Ret, *and* Gdnf *Expression*

Quantitative real-time polymerase chain reaction (PCR) analysis performed at E13.5 showed that *Gfra1* messenger RNA (mRNA) levels were reduced by 75%–80% in the kidneys, stomach, and duodenum of *Gfra1*$^{hypo/hypo}$ mice; expression levels decreased further toward the colon, where *Gfra1* mRNA levels were reduced by approximately 90% compared with control animals (Figure 1*E*). *Ret* mRNA levels were normal in the stomach and duodenum, but sharply decreased in the ileum of *Gfra1*$^{hypo/hypo}$ mice. In the cecum and colon, *Ret* mRNA was not detectable in our analysis (Figure 1*E*). This was expected because in the developing gut *Ret* is expressed exclusively in ENCCs, whereas *Gfra1* is expressed both in ENCCs and in the surrounding mesenchyme.[16,32–34] As our parallel analysis showed, ENCCs in *Gfra1*$^{hypo/hypo}$ mice were missing distal from the midileum (see later).

Gdnf mRNA levels were slightly—albeit significantly—increased throughout the GI tract, possibly reflecting mechanistic compensation for the reduced expression of GDNF receptors (Figure 1*E*). Western blot analysis showed that the amount of GFRa1 protein in the gut segment from the duodenum to the ileum of *Gfra1*$^{hypo/hypo}$ mice was reduced by 75%–80% at E13.5 (Figure 1*F* and *G*). In the cecum and colon, GFRa1 protein was not detectable in our analysis. Kidney development in *Gfra1*$^{hypo/hypo}$ mice was generally normal (Figure 1*H* and *I*). Given the hypomorphic *Gfra1* mRNA and protein levels measured in these mice, we renamed the *Gfra1*$^{pu\Delta tk}$ allele the *Gfra1* hypomorphic (*Gfra1*^{hypo}) allele.

Homozygous Gfra1$^{hypo/hypo}$ *Mice Have Impaired Neuronal Progenitor Colonization and Develop Aganglionosis and Hypertrophic Fibers in the Colon*

Mice that lack *Gdnf*, *Gfra1*, or *Ret* expression lack enteric nerves distal to the stomach.[20–22] Moreover, experiments in which *Gfra1* or *Ret* expression was deleted under temporal control in the developing gut showed that GDNF/GFRa1/RET signaling regulates the migration, proliferation, differentiation, and survival of ENCCs, particularly in the distal gut, in a gene dose-dependent manner.[18,25] Consistent with these findings, innervation of the stomach in *Gfra1*$^{hypo/hypo}$ mice appeared normal at E13.5, and the number of neuronal progenitors decreased gradually toward the distal gut (Figure 2*A*). At E13.5, *Gfra1*$^{hypo/hypo}$ embryos lacked neuronal progenitors from the midileum onward (Figure 2*A*). In the developing gut, *Ret* is expressed exclusively in ENCCs, whereas *Gfra1* is expressed both in ENCCs and in the surrounding mesenchyme.[16,32–34] As shown in Figure 2*A*, neuronal progenitors in the distal gut in *Gfra1*$^{hypo/hypo}$ embryos are missing, explaining the observed craniocaudal reduction in *Gfra1* mRNA and the absence of *Ret* mRNA in the distal gut (Figure 1*E*). Similar innervation defects were observed at E15.5 (ie, 3–4 days before birth in mice) (Figure 2*F*).

Heterozygous *Gfra1* null-allele (*Gfra1*$^{wild\ type\ [WT]/knockout\ [KO]}$) mice, which had an approximate 50% reduction in GFRa1 expression, had reduced enteric neuron fiber density and defects in gut function measured ex vivo; however, they did not have reduced numbers of enteric neurons, and they did not develop symptoms of either HSCR or HAEC.[20,23,35] Our finding that a 70%–80% reduction in *Gfra1* expression caused long-segment HSCR suggests a threshold effect in GFRa1-mediated downstream signaling. In the developing gut, 2 forms of the GFRa1 protein are present—the membrane-associated glycosylphosphatidylinositol-anchored form and the extracellular soluble form; these 2 forms can function cooperatively in mediating GDNF signaling in ENCCs.[34] Because the concentration of a solute decreases steeply as a function of distance from the source, signaling via the soluble form of GFRa1 is likely to be particularly sensitive to decreased expression. We analyzed the concentration dependence of soluble GFRa1 on downstream signaling in an MG87 fibroblast model system that stably expressed both *Ret* and a luciferase gene that reflected the activity of mitogen-activated protein kinases,[36] a downstream target of RET signaling. We stimulated these cells with GDNF together with increasing concentrations of

soluble GFRa1 and measured a sharp response in RET downstream signaling within a relatively narrow GFRa1 concentration range of 1.35–6.75 nmol/L (Figure 2*B*). These results provide a possible explanation for the phenotype differences observed between *Gfra1*$^{WT/KO}$ and *Gfra1*$^{hypo/hypo}$ mice. In *Gfra1*$^{WT/KO}$ mice, the GFRa1 levels were within the effective range, whereas GFRa1 levels fell below the effective range in *Gfra1*$^{hypo/hypo}$ mice.

Long-segment HSCR is defined as aganglionosis proximal to the splenic flexure.[37] Another hallmark clinical feature of HSCR is the presence of extrinsic hypertrophic nerve fibers in the distal colon.[38–40] At E18.5, *Gfra1*$^{hypo/hypo}$ mice had varying-length aganglionic segments proceeding from the midcolon (long-segment HSCR) or even from the distal ileum (total colonic aganglionosis), and they had hypertrophic nerve fibers in the distal colon (Figure 2*C* and *D*).

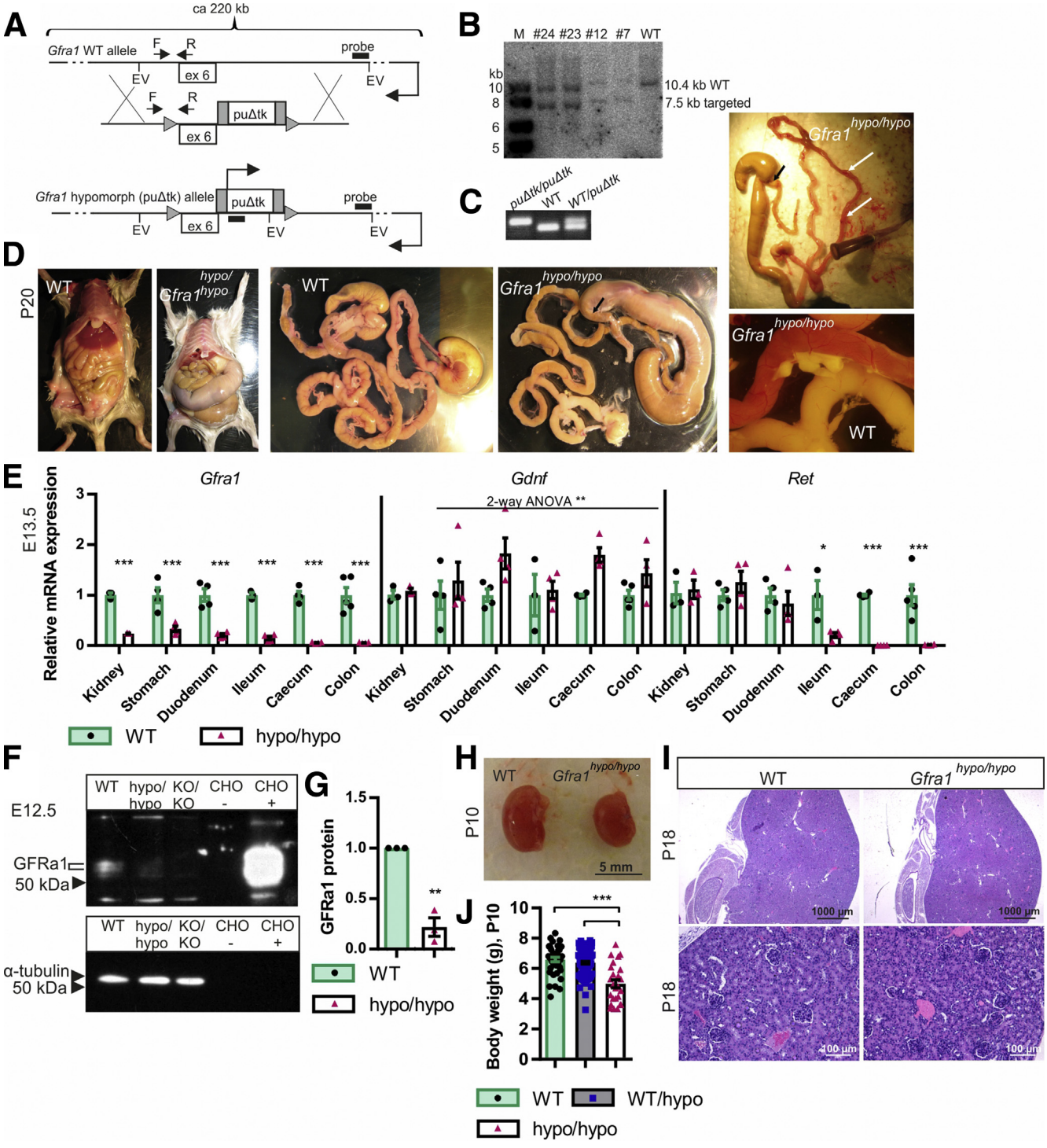

Because the presence of hypertrophic fibers in the colon of HSCR patients is diagnosed postnatally, we analyzed the colon in postnatal (P20) *Gfra1*$^{hypo/hypo}$ mice and found that the hypertrophic fibers still were present (Figure 2*E*).

Gfra1$^{hypo/hypo}$ mice are born with a normal appearance; however, they then develop symptoms that resemble HSCR, including constipation, distention of the gut, and a failure to thrive (Figure 1*J* and see later), with 100% penetrance by P10. Consistent with early mortality, the genotypes in the animal cohort were at the expected Mendelian ratios at E18.5, but not at P10 or P15–P23 (Table 1). Immunohistologic analysis of the ENS in *Gfra1*$^{hypo/hypo}$ mice at P10 using the pan-neuronal marker ubiquitin C-terminal hydrolase L1 showed normal ganglia in the duodenum, reduced ganglia size in the distal ileum, and absent or rudimentary ubiquitin C-terminal hydrolase L1-positive structures in the colon, reflecting hypertrophic fibers in the colon (Figure 3*A* and *B*). Similar results were obtained using the glial fibrillary acidic protein marker (Figure 3*C* and *D*). Collectively, results presented in Figures 2 and 3 are consistent with previous results on timed deletion of GFRa1 and RET until E18.5,[18,25] and suggest that reduced *Gfra1* expression in *Gfra1*$^{hypo/hypo}$ mice causes impaired craniocaudal colonization of the gut by enteric neuronal progenitors, with subsequent aganglionosis of the distal gut and the occurrence of hypertrophic nerve fibers in the distal colon.

Hypertrophic Fibers in the Colon of Gfra1$^{hypo/hypo}$ Mice Are Cholinergic

Hypertrophic nerve fibers in the distal colon of HSCR patients are known to be cholinergic.[40,41] The reduced flexibility of the aganglionic gut segment in HSCR patients is believed to result from excess extrinsic excitatory cholinergic stimuli and a lack of intrinsic inhibitory nitrergic stimuli.[42,43] To examine the properties of the myenteric plexus in *Gfra1*$^{hypo/hypo}$ mice, we stained for acetylcholinesterase. Our analysis showed that *Gfra1*$^{hypo/hypo}$ mice have normal cholinergic innervation in the duodenum and proximal ileum, reduced cholinergic innervation in the distal ileum, a lack of cholinergic innervation in the midcolon, and hypertrophic cholinergic fibers in the distal colon (Figure 4*A* and *B*). Next, we stained the myenteric plexus for reduced nicotinamide adenine dinucleotide phosphate (NADPH) diaphorase, a marker of nitric oxide synthase–positive nitrergic enteric neurons. Our analysis showed that *Gfra1*$^{hypo/hypo}$ mice have normal numbers of NADPH-diaphorase–positive neurons in the duodenum, but a complete lack of NADPH-diaphorase–positive cells in the distal colon (Figure 4*C* and *D*), reminiscent of the histopathologic findings in patients with HSCR.[42,43]

Histopathologic Characterization of HSCR/HAEC in Gfra1$^{hypo/hypo}$ Mice

Improving our understanding of the histopathologic changes that occur in HAEC may eventually help in developing more effective treatments. We used the histopathologic grading system for HAEC developed by Teitelbaum et al[7] to analyze *Gfra1*$^{hypo/hypo}$ mice. Teitelbaum et al[7] scored the histopathologic findings in HAEC in patients as follows: 0, no abnormalities; I, crypt dilatation and mucin retention; II, cryptitis or 2 crypt abscesses per high-power field; III, more than 2 crypt abscesses per high-power field; IV, fibrinopurulent debris and mucosal ulceration; and V, transluminal necrosis or perforation. However, compared with patients, mice with HAEC had milder infiltration of inflammatory cells into the crypts (milder cryptitis and crypt abscesses),[44] although the epithelial pathologies were similar (see later); therefore, we modified the grading system to primarily reflect epithelial pathology (see the Materials and Methods section). Another characteristic feature associated with HAEC is an overproduction of mucus and the retention of mucus in the colon, as well as a shift from producing acidic mucins to producing neutral mucins.[5,7] Mucins are produced primarily by goblet cells and form a protective barrier preventing bacterial enterocyte adherence.[45] Goblet cell hyperplasia[46] and altered goblet cell function[47] have been reported in HSCR.

Figure 1. (***See previous page***). **Generation of GFRa1 hypomorphic mice and analysis of Gfra1 expression.** (*A*) The *Gfra1* hypomorphic allele was generated by inserting a puΔtk cassette[31] into intron 6 in the *Gfra1* gene. (*B*) Representative Southern blot analysis of *Eco*RV-digested genomic DNA isolated from embryonic stem cells, confirming correct targeting of *Gfra1* via homologous recombination (expected sizes: targeted, 7564 bp; WT, 10397 bp). (*C*) PCR-based genotyping of mice using the primers indicated in panel *A* by F and R (expected sizes: WT, 88 bp; Gfra1$^{puΔtk/puΔtk}$, 100 bp). (*D*) *Gfra1*$^{hypo/hypo}$ mice develop megacolon, constipation, and abdominal distention, and they fail to thrive (note that the *Gfra1*$^{hypo/hypo}$ mouse is smaller than the WT mouse). The point of dilation is indicated by *black arrows*. At P18–P25, 50% of *Gfra1*$^{hypo/hypo}$ mice, sacrificed due to obvious discomfort due to abdominal swelling, have clearly visible acute erythema/hyperemia in the gastrointestinal tract (*white arrows*) indicative of enterocolitis; representative images are shown. (*E*) Relative *Gfra1*, *Gdnf*, and *Ret* mRNA levels at E13.5 in the indicated organs measured using qPCR (N = 4). (*F* and *G*) Western blot analysis of GFRa1 protein in the gut segment spanning from the duodenum to the ileum in E12.5 embryos. (*F*) Representative Western blot (samples obtained from E12.5 *Gfra1* KO mice were included as a negative control); (*G*) normalized average GFRa1 intensity (N = 3 independent experiments). (*H*) At P10, the kidneys in *Gfra1*$^{hypo/hypo}$ mice appear anatomically normal. (*J*) *Gfra1*$^{hypo/hypo}$ mice are smaller than WT and heterozygous littermates at P10 ($P < .001$). The slight reduction in kidney size in the *Gfra1*$^{hypo/hypo}$ mice likely reflects an overall failure of the mice to thrive. (*I*) Compared with WT littermates, kidney histology is grossly normal in P18 *Gfra1*$^{hypo/hypo}$ mice. F, forward primer; R, reverse primer; EV, *Eco*RV site; ex 6, exon 6; puΔtk/puΔtk, *Gfra1*$^{puΔtk/puΔtk}$; KO/KO, *Gfra1*$^{KO/KO}$; CHO, Chinese hamster ovary cells transfected with a plasmid encoding GFP (-) or Gfra1 (+). All summary data are presented as means ± SEM. *$P < .05$, **$P < .01$, and ***$P < .001$. Statistical analyses were performed using the Student *t* test, unless indicated otherwise.

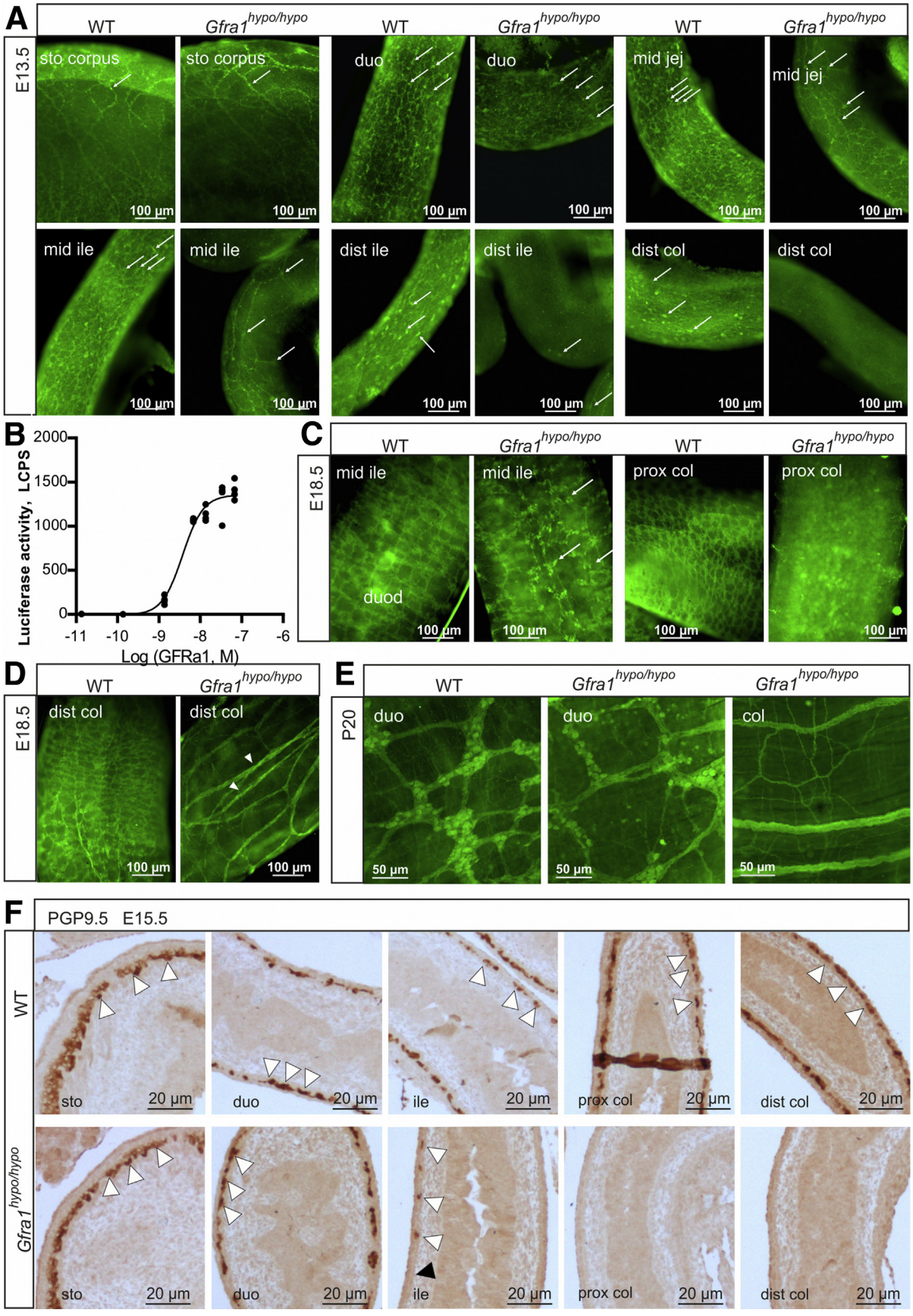
A
WT
Gfra1hypo/hypo
WT
Gfra1hypo/hypo
WT
Gfra1hypo/hypo
E13.5
sto corpus
sto corpus
duo
duo
mid jej
mid jej
mid ile
mid ile
dist ile
dist ile
dist col
dist col
100 µm
B
Luciferase activity, LCPS
2000
1500
1000
500
0
-11
-10
-9
-8
-7
-6
Log (GFRa1, M)
C
WT
Gfra1hypo/hypo
WT
Gfra1hypo/hypo
E18.5
mid ile
mid ile
prox col
prox col
duod
100 µm
D
WT
Gfra1hypo/hypo
E18.5
dist col
dist col
100 µm
E
WT
Gfra1hypo/hypo
Gfra1hypo/hypo
P20
duo
duo
col
50 µm
F
PGP9.5 E15.5
WT
Gfra1hypo/hypo
sto
duo
ile
prox col
dist col
20 µm

Table 1. Distribution of Offspring Genotypes Born From Breedings Between *Gfra1*$^{wt/hypo}$ Animals

		Distribution, number of animals (% total)	Expected, number of animals (% total)
E18.5	WT	27 (25.23)	26.75 (25)
$P = .308$	WT/hypo	59 (55.14)	53.5 (50)
	Hypo/hypo	21 (19.63)	26.75 (25)
P10	WT	39 (24.38)	35.75 (25)
$P = .018$	WT/hypo	96 (60.00)	71.5 (50)
	Hypo/hypo	25 (15.63)	35.75 (25)
P15–P23	WT	37 (35.24)	26.25 (25)
$P < .001$	WT/hypo	60 (57.14)	52.5 (50)
	Hypo/hypo	8 (7.62)	26.25 (25)

NOTE. At E18.5, *Gfra1*$^{hypo/hypo}$ mice are present at the expected Mendelian ratio, but not at P10 ($P < .05$) or at P15–P23 ($P < .001$), chi-square analysis.

Histopathologic characterization of HSCR/HAEC in E18.5, P4, and P10 Gfra1$^{hypo/hypo}$ *mice.* Histologic analysis of the colon in E18.5 *Gfra1*$^{hypo/hypo}$ mice showed no overt changes compared with control mice (Figure 5*A* and *B*). However, at P4, histologic analysis using Alcian blue (AB), periodic acid–Schiff (PAS), H&E, and Gram staining showed from minimal to moderate epithelial damage accompanied by crypt dilatation and a mucin shift from acidic to neutral with mucus retention in the goblet cells (Figure 5*C*–*F*, Table 2). At P10 the differences were more advanced: slight to mild multifocal to diffuse epithelial hyperplasia, as well as dysplasia (ie, disorganization) accompanied by degeneration of surface colonocytes in *Gfra1*$^{hypo/hypo}$ mice (Figures 6*A* and *B*) was observed, indicating mild surface epithelial damage. In the hyperplastic and degenerated areas of the colon, the epithelial cells grew in disorganized, undulating rows with partly overlapping nuclei (Figure 6*B* and *C*). In addition, the crypts in the colon were mildly to moderately dilated with various degrees of mucin retention (Figure 6*B* and *C*), indicating an overproduction and retention of mucus in the colon. We also observed increased numbers of intraepithelial apoptotic cell remnants in 5 of 8 *Gfra1*$^{hypo/hypo}$ mice, indicating a degenerative process (Figure 6*B*). Importantly, the severity of these features varied between animals (the histopathologic data from each animal are presented in Table 3).

At P10, goblet cell pathology was more advanced, with a further shift in mucin production from acidic to neutral now also accompanied by goblet cell hyperplasia in all mutant mice. Notably, the earlier-described goblet cell pathology appeared in all mice regardless of the extent of the aforementioned epithelial pathology (Figure 6*C*, Table 3). More specifically, we observed that PAS-positive goblet cells, which are normally found in the apical and central parts of the crypts, were present at the base of the crypts in the *Gfra1*$^{hypo/hypo}$ colon (Figure 6*B* and *C*). On the other hand, AB, which stains acidic mucins, showed that AB-positive goblet cells, which are normally found at the base of crypts, are either absent or filled with a foamy mixture of both neutral and acidic mucins in the *Gfra1*$^{hypo/hypo}$ colon (Figure 6*B* and *C*; Table 3). To gain insight into whether altered goblet cell physiology in the *Gfra1*$^{hypo/hypo}$ colon results from a deficit in the ENS in the colon and distal intestine, or from a reduction in GFRa1 levels in fetal mesenchyme in the whole intestine, we also analyzed goblet cells in the duodenum at P10 using AB-PAS staining. The number of goblet cells and the mucin profile were unchanged in the duodenum at P10 (Figure 6*F*–*H*).

Finally, both Gram and H&E staining showed no evidence of bacterial enterocyte adherence or microbial infection in the *Gfra1*$^{hypo/hypo}$ colon at P10 (Table 3). Based on our histopathologic grading system of HAEC, 3 of the 8 *Gfra1*$^{hypo/hypo}$ mice at P10 had a grade III HAEC score, 4 mice had a grade II HAEC score, and 1 mouse had a grade I HAEC score.

Taken together, these results suggest that a mucin shift from acidic to neutral in goblet cells at P4 is further

Figure 2. (***See previous page***). **Impaired enteric neuronal progenitor colonization and hypertrophic nerve fibers in the distal gut of GFRa1 hypomorphic mice.** (*A*) Immunohistochemistry using the pan-neuronal marker ubiquitin C-terminal hydrolase L1 in E13.5 WT and *Gfra1*$^{hypo/hypo}$ mice whole-mount GI tract preparations. Note the reduced numbers of neuronal progenitors (*white arrows*) beginning at the midjejunum of *Gfra1*$^{hypo/hypo}$ mice and the absence of neuronal progenitors from the distal and GDNF ileum onward; representative images are shown (N = 3–4 animals per genotype). (*B*) Dose-dependent activation of mitogen-activated protein kinase signaling by soluble GFRa1. MG87 fibroblasts stably expressing RET and the PathDetect Elk-1 luciferase system were treated with the indicated concentration of soluble GFRa1 (N = 4 biological replicates per experiment; N = 2 experiments). (*C* and *D*) ubiquitin C-terminal hydrolase L1 immunohistochemistry was performed in E18.5 WT and *Gfra1*$^{hypo/hypo}$ mice from whole-mount GI tract preparations, showing reduced and scattered innervation in the midileum, an absence of innervation in the proximal colon, and hypertrophic fibers in the distal colon (*white arrowheads*, a hallmark feature of HSCR); the *white arrows* indicate neuronal somas. Representative images are shown (N = 3–4 animals per genotype). (*E*) ubiquitin C-terminal hydrolase L1 immunohistochemistry performed on P20 whole-mount myenteric plexus preparations showing normal innervation in the duodenum, an absence of neuronal cell bodies in the colon, and hypertrophic fibers in the colon of *Gfra1*$^{hypo/hypo}$ mice; representative images are shown (N = 2–3 animals per genotype). (*F*) The ENCC colonization of the mouse hindgut is complete by E14.5. Representative image of sagittal gut sections immunostained with the pan-neuronal marker ubiquitin C-terminal hydrolase L1 in E15.5 WT and *Gfra1*$^{hypo/hypo}$ mice, showing that the enteric neuronal progenitors have reached the distal colon in the WT mice (*white arrowheads*); in contrast, enteric neuronal progenitors reached the proximal ileum (*white arrowheads*) in E15.5 *Gfra1*$^{hypo/hypo}$ mice, but are absent from the distal ileum, cecum, and colon. The point at which aganglionosis begins is indicated by a *black arrowhead*; representative images from WT and *Gfra1*$^{hypo/hypo}$ mice are shown. dist, distal; duo, duodenum; ile, ileum; jej, jejunum; prox, proximal.

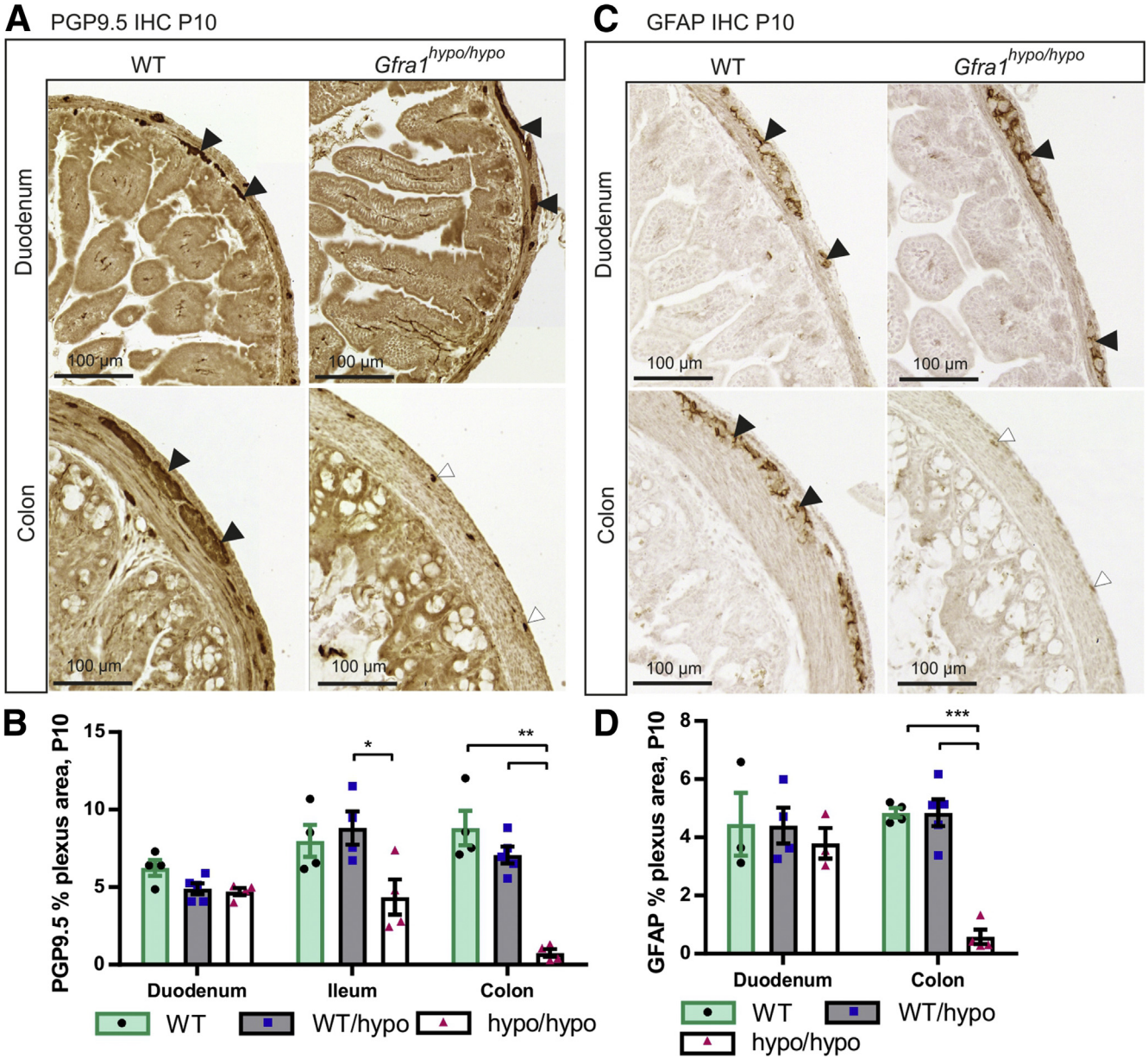

Figure 3. Analysis of the enteric nervous system in P10 Gfra1 hypomorphic mice. (*A*) Representative images of the pan-neuronal marker ubiquitin C-terminal hydrolase L1 immunohistochemistry in coronal gut sections prepared from P10 mice. (*B*) Quantification of the ganglionated plexus area (*black arrowheads* in *A*) in P10 WT and *Gfra1*$^{hypo/hypo}$ coronal gut sections; the residual staining in the *Gfra1*$^{hypo/hypo}$ mice colon reflects hypertrophic fibers or transition zone (*white arrowheads* in *A*). $P < .05$ *Gfra1*$^{WT/hypo}$ vs *Gfra1*$^{hypo/hypo}$ in ileum and $P < .01$ WT and *Gfra1*$^{WT/hypo}$ vs *Gfra1*$^{hypo/hypo}$ in colon, N = 4–5 mice per genotype. Analysis of variance and the Tukey multiple comparisons tests were used for statistical analysis. (*C*) Immunostaining for the glial marker, glial fibrillary acidic protein (GFAP), in the duodenum of P10 mice is similar between genotypes (N = 3; representative images are shown). *Black arrowheads* indicate ganglia stained with GFAP, *white arrowheads* mark residual staining from hypertrophic fibers of the transition zone. Reminiscent of the results obtained using ubiquitin C-terminal hydrolase L1 at the same age (*A* and *B*) in the colon, Gfra1$^{hypo/hypo}$ mice have a smaller GFAP-positive plexus area in the myenteric plexus relative to littermate controls quantified in panel *D*; N = 4–5 animals per genotype; $P < .001$, analysis of variance and the Tukey multiple comparisons test (data are presented as means ± SEM). All summary data are presented as means ± SEM. *$P < .05$, **$P < .01$, and ***$P < .001$.

enhanced and accompanied with hyperplasia at P10 and that those are generally ubiquitous early events in *Gfra1*$^{hypo/hypo}$ mice. On the other hand, the interanimal variations in epithelial damage, epithelial degeneration, crypt dilatation, and mucin retention (Table 3) suggest that these changes may be secondary to goblet cell dysfunction and appear later in HAEC.

Histopathologic characterization of HSCR/HAEC in P18–P25 Gfra1$^{hypo/hypo}$ *mice.* To analyze the features of advanced HAEC in our *Gfra1*$^{hypo/hypo}$ mice, we examined

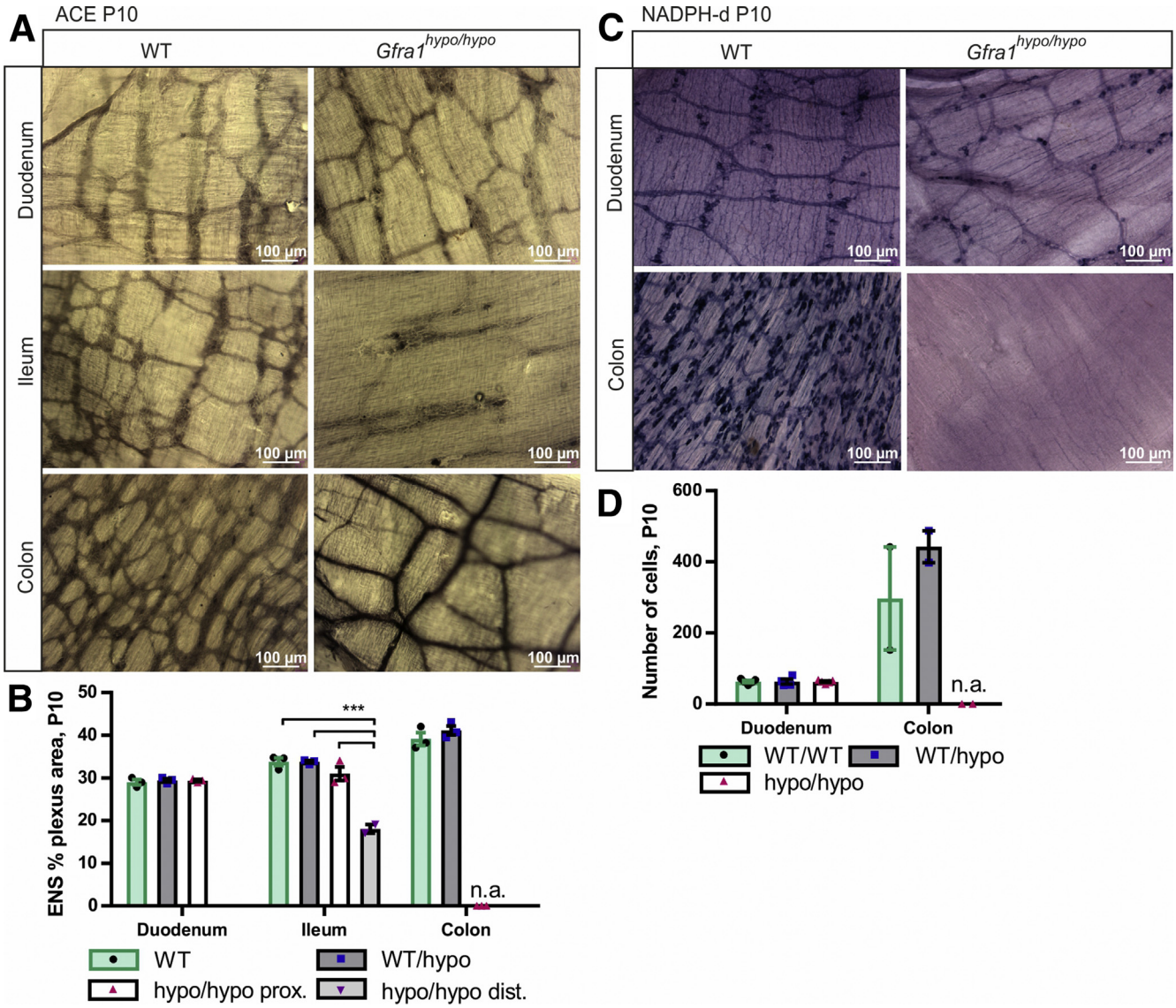

Figure 4. The hypertrophic nerve fibers in the distal gut of GFRa1 hypomorphic mice are cholinergic. (*A*) Acetylcholinesterase histochemistry at P10 showing similar innervation in the duodenum, as well as cholinergic hypertrophic nerve fibers characteristic of HSCR in the colon of *Gfra1*$^{hypo/hypo}$ mice. In the ileum, an image distal of the point of dilatation is shown (N = 3 animals per genotype). (*B*) Quantification of the acetylcholinesterase-positive plexus area in P10 WT and *Gfra1*$^{hypo/hypo}$ mice (N = 3 animals per genotype, ***$P < .001$). (*C*) NADPH diaphorase histochemistry for nitric oxide synthase (NOS)-positive neurons in P10 mice showing similar innervation in the duodenum and an absence of NOS-positive innervation in the colon of *Gfra1*$^{hypo/hypo}$ mice; N = 4–5 animals per genotype (N = 2 animals per genotype for the colon). (*D*) Quantification of NOS-positive plexus area in P10 WT and *Gfra1*$^{hypo/hypo}$ mice; N = 4–5 animals per genotype (N = 2 animals per genotype for the colon). Analysis of variance and the Tukey multiple comparisons tests were used for statistical analysis. n.a., not applicable for *Gfra1*$^{hypo/hypo}$ mice. ACE, acetylcholinesterase; dist, distal; prox, proximal (data are presented as means ± SEM). All summary data are presented as means ± SEM. *$P < .05$, **$P < .01$, and ***$P < .001$.

P18–P25 mice that showed obvious signs of discomfort, including cachexia, abdominal swelling, and reduced spontaneous activity. In these mice, we observed histopathologic features that are reminiscent of advanced HAEC in HSCR patients[5–7] (Figures 7 and 8; Table 4). Compared with P10 mice, in all animals analyzed the P18–P25 mice had more advanced levels of leukocyte accumulation, epithelial damage (including the presence of apoptotic cell remnants), mucus accumulation, and crypt dilatation–associated edema (Figures 6–8; Tables 3 and 4). The shift from acidic to neutral mucin production observed at P10 also clearly was evident at P18–P25 (Figure 7). Moreover, goblet cell hyperplasia (Figure 7*B* and *C*) was present only in mice with moderate epithelial damage; in contrast, mice with marked epithelial damage had either degenerated goblet cells or a combined phenotype of goblet cell hyperplasia and goblet cell degeneration (Figures 7*C* and 8*B*; Table 4). A variety of other features that are typical in advanced HAEC, including ulceration, necrotic purulent colitis, crypt abscesses, and/or the presence of focal bacterial aggregates, were observed in

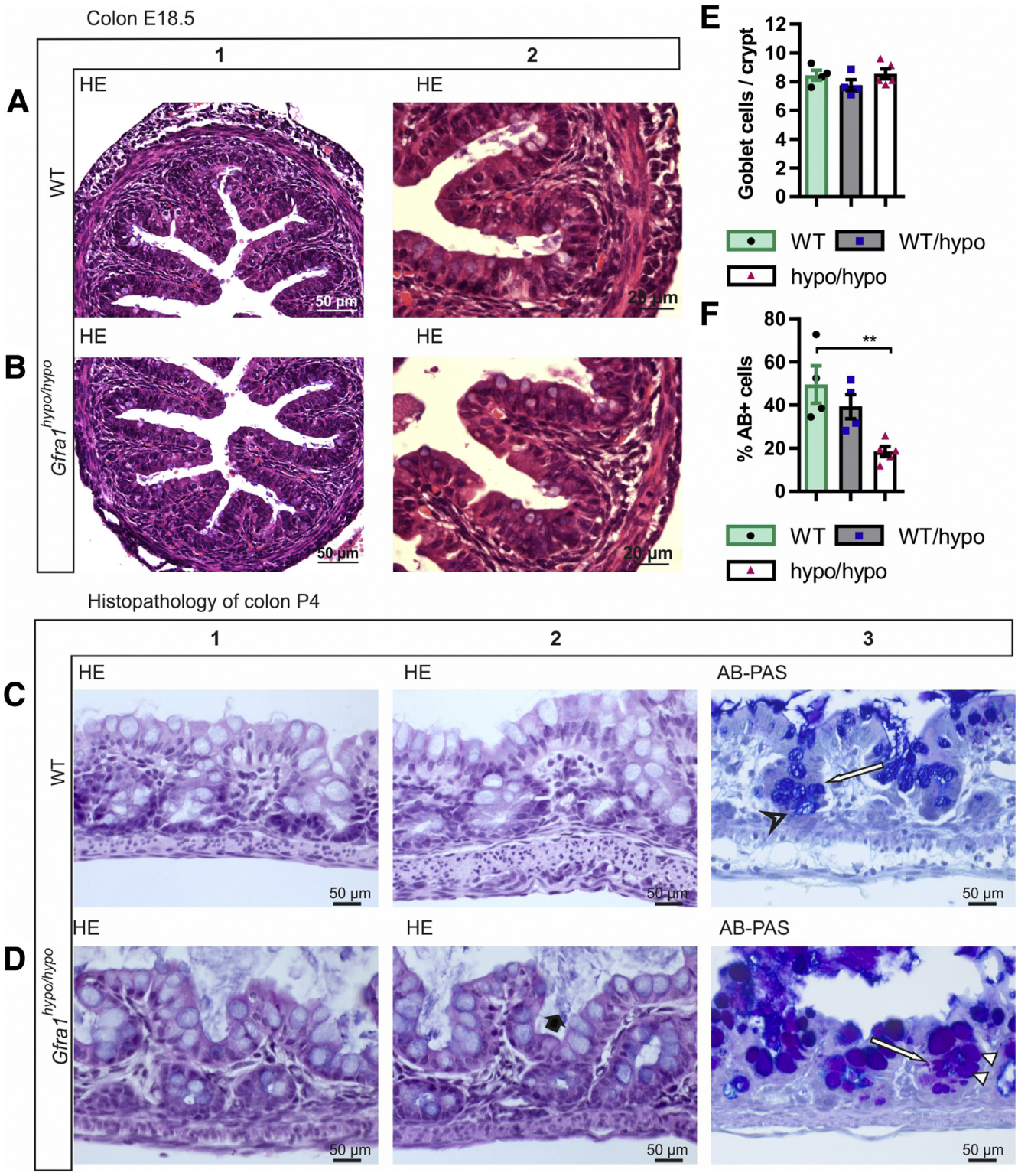

Figure 5. Histopathology of colon at E18.5 and P4. (*A* and *B*) Representative H&E-stained coronal sections of the colon at E18.5. No gross difference was observed between genotypes (N = 3–4 animals per genotype). (*C* and *D*). H&E staining from WT and *Gfra1*$^{hypo/hypo}$ colon at P4. *Gfra1*$^{hypo/hypo}$ animals typically show mild crypt dilatation accompanied with mucus retention (*D2*, *black bold arrow*). AB-PAS staining shows more acidic mucins in WT animals at the basal crypts (*C*3, *open arrowhead*) and more neutral mucins in *Gfra1*$^{hypo/hypo}$ animals (*white arrowheads*) quantified in *F*. $^{**}P < .01$ (N = 3–4). (*E*) The number of goblet cells (*C*3 and *D*3, *white arrows*) was not changed at P4 (N = 4–5). Analysis of variance and the Tukey multiple comparisons test, data are presented as means ± SEM. All summary data are presented as means ± SEM.

Table 2. Summary of Histopathologic Findings at P4

P4	ID	Weight, *g*	Sex	Applied Teitelbaum et al[7] grade	Surface epithelial injury	Crypt dilation	Intraepithelial apoptotic remnants	Goblet cell hyperplasia	Mucins in crypts				Bacteria in crypts	Enterocyte adherence	Leukocytes	
									Mucin shift to PAS	Basal	Surface	Mucus retention			Granulocytes	Lymphocytes
WT	7615-2	3.02	F	0	-	-	-	No	No	AB	PAS	-	-	No	-	-
WT	7640-3	2.96	F	0	-	-	-	No	No	AB	PAS	-	-	No	-	-
WT	7640-4	3.16	M	0	-	-	-	No	No	AB	PAS	-	-	No	-	-
WT	7640-4a	2.92	M	0	-	-	-	No	No	AB	PAS	-	-	No	-	-
WT/hypo	7615-4	3.15	F	0	-	-	-	No	No	AB	PAS	-	-	No	-	+
WT/hypo	7615-1	3.21	F	0	-	-	-	No	No	AB	PAS	-	-	No	-	-
WT/hypo	7615-5	3.06	M	0	-	-	-	No	No	AB	PAS	-	-	No	-	-
WT/hypo	7640-5a	2.78	M	0	-	-	-	No	No	AB	PAS	-	-	No	-	-
Hypo/hypo	7615-3	2.60	F	I	Mild	++	-	No	Yes	PAS	PAS	++	-	No	-	-
Hypo/hypo	7640-1	2.38	F	I	Mild	++	-	No	Yes	PAS	PAS	++	-	No	-	-
Hypo/hypo	7640-1a	2.34	M	I	Mild	+++	-	No	Yes	PAS	PAS	++	-	No	-	-
Hypo/hypo	7640-3a	2.44	M	I	Minimal	+	-	No	Yes	PAS	PAS	++	-	No	-	-
Hypo/hypo	7640-2	2.51	M	II	Moderate	++	+	No	Yes	PAS	PAS	++	-	No	-	-
					Minimal	Mild +	Mild +					Mild +	Mild +		Normal - (<4/HPF)	
				0–V	Mild	Moderate ++	Moderate ++	Yes/no	Yes/no			Moderate ++	Moderate ++	Yes/no	Mild + (5–15/HPF)	
					Moderate	Marked +++	Marked +++					Marked +++			Moderate ++ (20–30/HPF)	
					Marked											

NOTE. See the Materials and Methods section for details regarding the histopathologic grading.

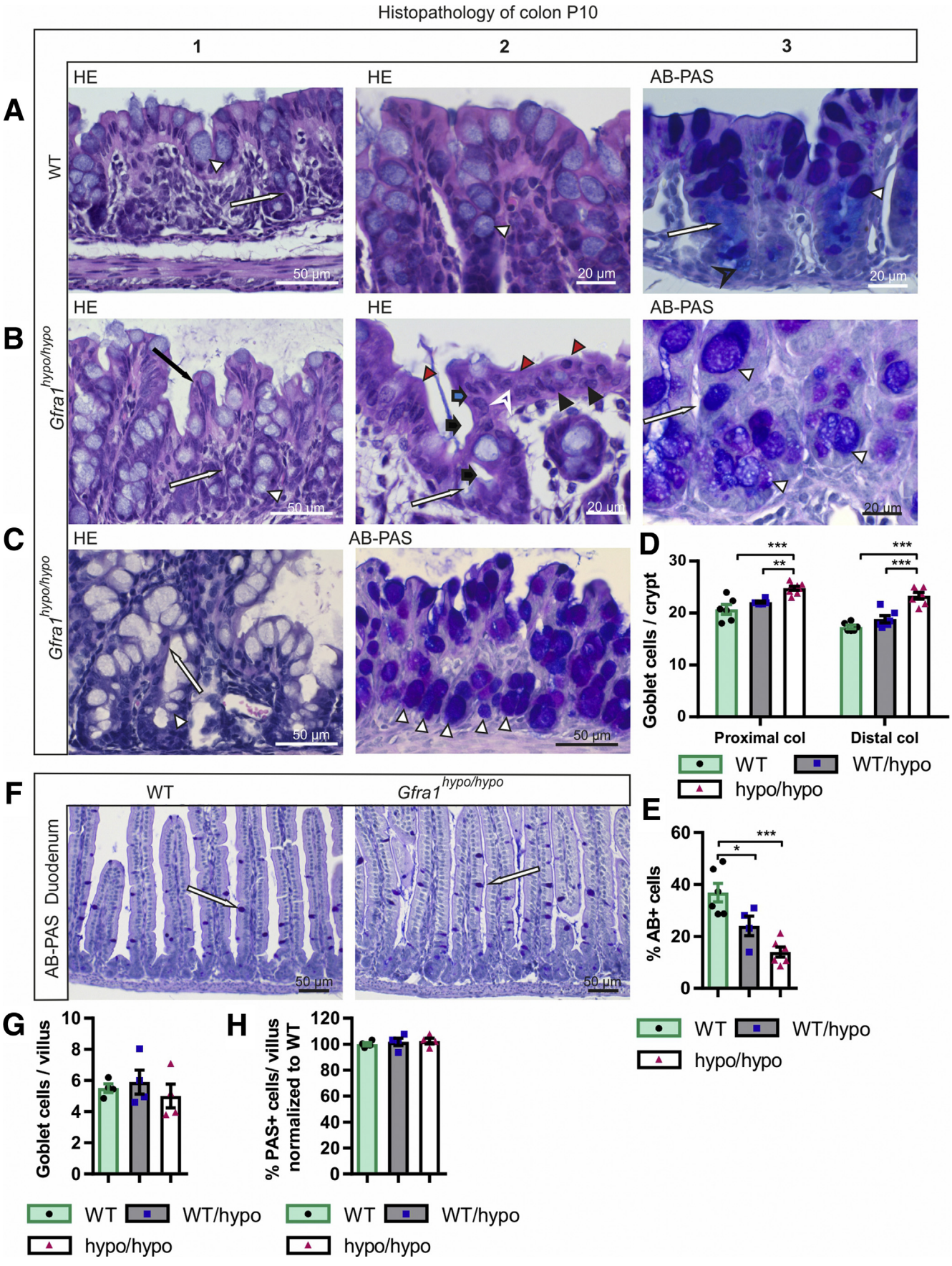
Histopathology of colon P10
1
2
3
A
B
C
WT
Gfra1 hypo/hypo
HE
AB-PAS
50 µm
20 µm
D
Goblet cells / crypt
Proximal col
Distal col
WT
WT/hypo
hypo/hypo
E
% AB+ cells
F
AB-PAS Duodenum
G
Goblet cells / villus
H
% PAS+ cells/ villus normalized to WT

3 of the 4 animals investigated (Figure 7*D* and *E*). Bacterial enterocyte adherence on the other hand was observed in only 2 of the 3 mice with severe epithelial damage (Table 4); these same 2 mice also had bacteria within the colon crypts and blood vessels (Figures 7*D* and *E* and 8*B* and *C*), indicating sepsis. The histopathologic findings of each mouse examined at P4, P10, or P18–P25 are summarized in Tables 2, 3, and 4, respectively.

Taken together, these data suggest that *Gfra1*$^{hypo/hypo}$ animals recapitulate both the early and advanced histopathologic findings present in patients with HAEC.[4,5,7]

Characterization of Cytokine mRNA Expression and Serum Protein Levels in Gfra1$^{hypo/hypo}$ Mice

A mouse long-segment HSCR/HAEC model may allow identification of diagnostic markers and further explore the relationship between immune response and HAEC. As a first step in this direction we analyzed the expression of mRNAs for *Il1a*, *Il1b*, *Il1Ra*, *Il2*, *Il4*, *Il5*, *Il6*, *Il10*, *Il13*, *Il23*, *Tgfb1*, *Tnf*, and *Ifng* selected based on their presumed or hypothetical involvement in GI tract inflammation. First, we performed a pilot study on mRNA expression in the colon at P10, when the HSCR/HAEC phenotype is readily detectable but less variable than at the end stage of the disease. Of 13 selected mRNAs, 7 were detectably expressed at P10 (Figure 9*A*). Based on those preliminary results *Tnf*, *Il1b*, and *Tgfb1* mRNA were selected for further analysis at E18,5, P5, and P12–P15, while the n number of animals analyzed at P10 was increased. We observed moderate 2- to 3-fold up-regulation of *Tnf* at P5 and P10 in the colon of *Gfra1*$^{hypo/hypo}$ animals (Figure 9*B*). *Il1b* mRNA expression showed increased expression in *Gfra1*$^{hypo/hypo}$ mice with remarkable interanimal variation (Figure 9*C*). Expression levels of *Tgfb1* were similar between genotypes (Figure 9*D*). The downward trend in *Tnf* and *Il1b* mRNA expression in older animals may reflect the fact that more severely affected individuals die before P10 (Table 1). The observed peak in *Tnf* and *Il1b* mRNA expression in a few animals therefore may reflect the end stage of the disease, which is associated with acute bacterial enterocyte attachment, tissue invasion, and sepsis.

In the small intestine we were unable to detect significant differences in *Tnf* and *Il1b* mRNA expression (Figure 9*E* and *F*).

We also analyzed cytokine interferon γ, interleukin (IL) 12, IL4, IL5, IL6, tumor necrosis factor (TNF), IL1b, and IL9 protein levels in the serum using commercially available enzyme-linked immunosorbent assay (ELISA) analysis tools at P10 and P14–P16. We were able to detect TNF, IL5, and IL6 with no clear genotype–phenotype correlation (Figure 9*H* and *I*). We hypothesized that systemic immune activation with notable serum cytokine changes in the *Gfra1*$^{hypo/hypo}$ HSCR/HAEC mouse model was a late event that was associated with bacterial invasion and sepsis at the end stage.

Discussion

Here, we report that reducing GFRa1 expression in mice does not affect renal development, but is sufficient to cause a long-segment HSCR-like phenotype. Why is ENS development in heterozygous *Gfra1*$^{WT/KO}$ mice grossly normal, whereas homozygous *Gfra1*$^{hypo/hypo}$ mice, which have only a 20%–30% further reduction in GFRa1 levels compared with *Gfra1*$^{WT/KO}$ mice, develop HSCR? Our results using a reporter cell line suggest that GFRa1 levels need to exceed a specific threshold before downstream signaling is activated. It is possible that during ENS development this threshold level of GFRa1 in *Gfra1*$^{hypo/hypo}$ mice is not reached. Previous attempts to alter GDNF/GFRa1/RET signaling by introducing knock-in alleles for *Ret* led to defects in both the ENS and kidneys.[24] It is possible that the level of RET phosphorylation required for normal development is higher in the developing ENS compared with the developing kidneys. GDNF and GFRa1 also can promote synapse formation in a

Figure 6. (*See previous page*). Mild epithelial damage, mucin retention, mucin type changes, and goblet cell hyperplasia in P10 *Gfra1*$^{hypo/hypo}$ mice. (*A*1–2) H&E and AB-PAS (*A*3) staining of coronal colon sections from P10 WT mice. In WT mice, the mucosa is thin and compact with an evenly palisading, regular surface epithelium. The crypts of Lieberkühn (*A*1 and *A*3, *white arrow*) in the colon are shallow and straight. Goblet cells (*A*1–3, *white arrowhead*) are abundant in surface epithelium and within the proximal third of the crypts, but less abundant at the crypt bases (*A*3). The goblet cells in the surface epithelium and in the proximal parts of the crypts contain PAS-positive neutral mucins, staining deep purple (*A*3, *white arrowhead*). The goblet cells in the basal parts of the crypts primarily contain AB-positive acidic droplets, staining light blue (*A*3, *black open arrowhead*). (*B* and *C*) In *Gfra1*$^{hypo/hypo}$ mice, the colon crypts (*B*1, *B*3, and *C*1, *white arrow*) are mildly to moderately dilated, with variable levels of mucin retention (*B*2, *black bold arrow*). The surface of the mucosa in the colon of *Gfra1*$^{hypo/hypo}$ mice is bumpy in appearance (compare *A*1 with *B*1), and epithelial cells grow in disorganized, undulating rows with partly overlapping nuclei (*B*1, *black arrow*). The height variation of the epithelial cells (*B*2, *blue bold arrow*), the round to oval bland nuclei (*B*2, *black arrowhead*), increased eosinophilia in the apical cytoplasm (*B*2, *red arrowheads*), and the indistinct cell borders (*B*2, *white open arrowhead*) are indicative of degeneration and mild epithelial damage. Unlike in WT mice (*A*3), the goblet cells in *Gfra1*$^{hypo/hypo}$ mice often are abundant in the basal parts of the crypts (*C*2, *white arrowheads*) and show a shift toward the production of PAS-positive (ie, neutral) mucins (compare *C*2 with *A*3). (*D*) Quantification of goblet cells in WT, *Gfra1*$^{WT/hypo}$, and *Gfra1*$^{hypo/hypo}$ mice, for which the number of goblet cells is increased both in proximal ($P < .001$ and $P < .01$) and distal colons ($P < .001$) compared with both heterozygous and WT animals; N = 6–8 animals per genotype. (*E*) *Gfra1*$^{hypo/hypo}$ mice and *Gfra1*$^{WT/hypo}$ have fewer AB-positive cells per crypt compared with WT colon ($P < .001$ and $P < .05$, N = 4–5). (*F*) AB-PAS staining from WT and hypomorphic duodenum at P10. (*G*) Quantification of goblet cells (*F*, *white arrows*) in WT, *Gfra1*$^{WT/hypo}$, and *Gfra1*$^{hypo/hypo}$ mice in P10 duodenum (N = 4 per genotype). (*H*) Quantification of PAS-positive goblet cells, AB-positive goblet cells were absent in duodenum (N = 4 mice per genotype). $^{*}P < .05$, $^{**}P < .01$, and $^{***}P < .001$. col, colon. Analysis of variance and the Tukey multiple comparisons test, data are presented as means ± SEM. All summary data are presented as means ± SEM.

Table 3. Summary of Histopathologic Findings at P10

									Mucins in crypts					Leukocytes	
P10	ID	Weight, *g*	Sex	Applied Teitelbaum et al[7] grade	Surface epithelial damage	Crypt dilation	Intraepithelial apoptotic remnants	Goblet cell hyperplasia	Mucin shift to PAS	Basal	Surface	Mucus retention	Bacteria in crypts	Enterocyte adherence	Granulocytes	Lymphocytes
WT	10	6.8	F	0	-	-	-	No	No	AB	PAS	-	-	No	-	-
WT	23	5.3	M	0	-	-	-	No	No	AB	PAS	-	-	No	-	-
WT	6280-1	8	M	0	-	-	-	No	No	AB	PAS	-	-	No	-	-
WT	31	4.12	M	0	-	-	-	No	No	AB/PAS	PAS	-	-	No	-	-
WT/hypo	22	6.09	M	0	-	-	-	No	No	AB/PAS	PAS	-	-	No	-	-
WT/hypo	24	6.42	F	0	-	-	-	No	No	AB	PAS	-	-	No	-	-/+
WT/hypo	6777-3	5.18	M	0	-	-	-	No	No	AB	PAS	-	-	No	-	-
WT/hypo	6280-2	7.84	M	0	-	-	-	No	No	AB	PAS	-	-	No	-	-
WT/hypo	12	6.42	M	0-I	No/minimal	-	-	No	No	AB/PAS	PAS	-	-	No	-	-
Hypo/hypo	11	3.61	M	I	Minimal	-	-	Yes	Yes	PAS	PAS	-	-	No	-	-
Hypo/hypo	27	7.57	M	II	Mild	-	+	Yes	Yes	PAS	PAS	-	-	No	-	-
Hypo/hypo	6277-7	3.6	F	II	Mild	+/++	-	Yes	Yes	PAS	PAS	+	-	No	-	-
Hypo/hypo	21	4.93	F	III	Moderate	+	+	Yes	Yes	PAS	PAS	++	-	No	-	+
Hypo/hypo	6224-2	4.15	M	II	Mild	+	+	Yes	Yes	PAS	PAS + AB	+	-	No	-	-
Hypo/hypo	6224-7	5.93	F	III	Moderate	++	+	Yes	Yes	PAS	PAS + AB	+	-	No	++	-
Hypo/hypo	7310-1	4.53	M	III	Moderate	++	+	Yes	Yes	PAS/foamyAB	PAS/foamyAB	++	-	No	-	-
Hypo/hypo	7310-2	3.62	M	II	Mild	++/+++	-	Yes	Yes	PAS/foamyAB	PAS/foamyAB	++	-	No	-	-
					Minimal	Mild +	Mild +					Mild +	Mild +		Normal - (<4/HPF)	
				0–V	Mild	Moderate ++	Moderate ++	Yes/no	Yes/no			Moderate ++	Moderate ++	Yes/no	Mild + (5–15/HPF)	
					Moderate	Marked +++	Marked +++					Marked +++			Moderate ++ (20–30/HPF)	
					Marked											

NOTE. See the Materials and Methods section for details regarding the histopathologic grading.

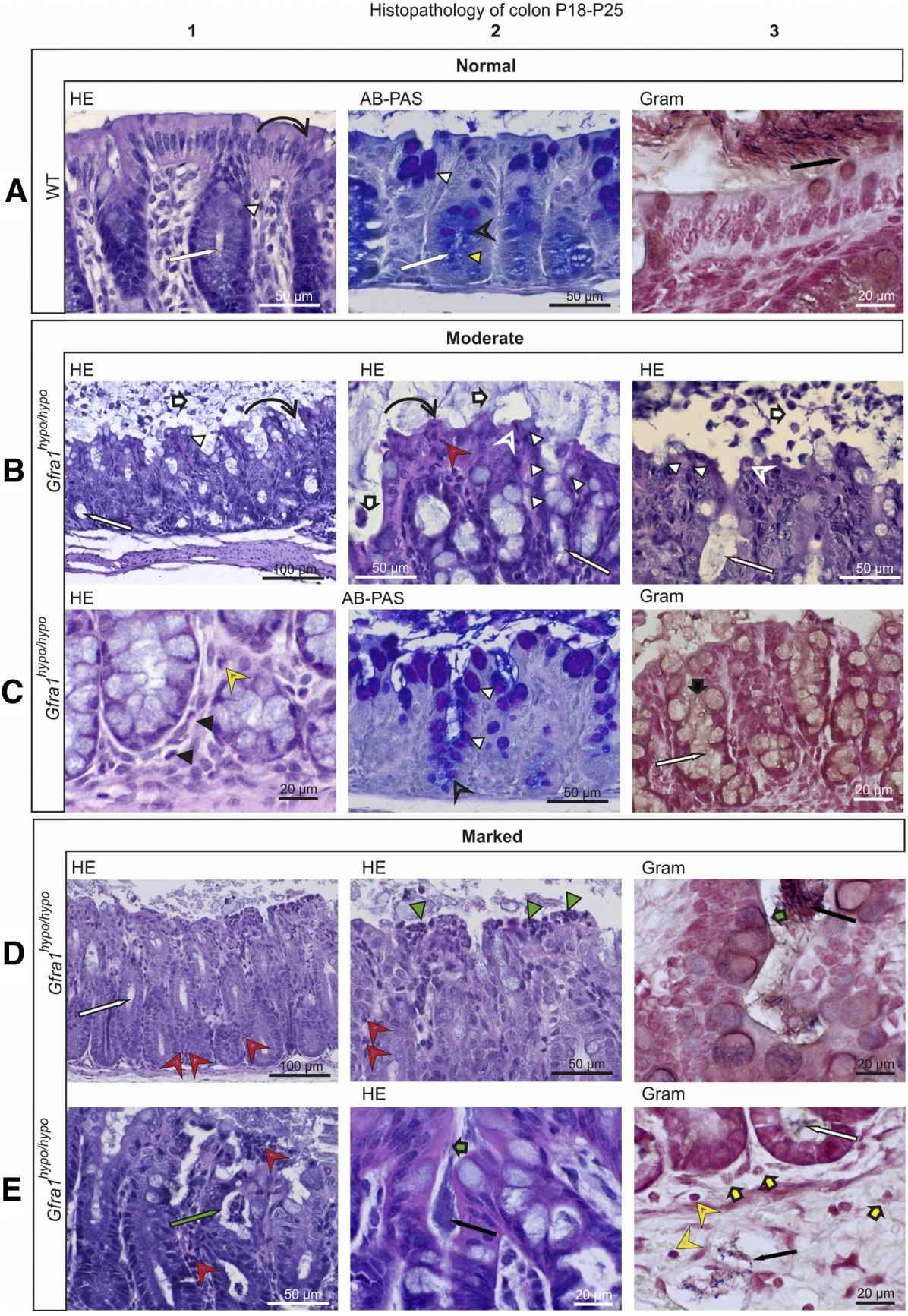
Histopathology of colon P18-P25
1
2
3
A
WT
Normal
HE
AB-PAS
Gram
50 µm
50 µm
20 µm
B
Gfra1hypo/hypo
Moderate
HE
HE
HE
100 µm
50 µm
50 µm
C
Gfra1hypo/hypo
HE
AB-PAS
Gram
20 µm
50 µm
20 µm
D
Gfra1hypo/hypo
Marked
HE
HE
Gram
100 µm
50 µm
20 µm
E
Gfra1hypo/hypo
HE
Gram
50 µm
20 µm
20 µm

RET-independent manner via a process called *ligand-induced cell adhesion*, which also may influence cell migration,[48] and therefore synapse formation could be another process in which a reduction in GFRa1 levels may impact ENS development differently from the kidneys. Unfortunately, methods for quantifying RET phosphorylation in vivo are not currently available, thus precluding the ability to quantify RET signaling to discriminate between RET-dependent from RET-independent effects in ENS and kidney development.

Our *Gfra1*$^{hypo/hypo}$ mouse provides an opportunity to model childhood HSCR and HAEC arising from a defect in the GDNF/GFRa1/RET signaling axis. At 10 days of age, *Gfra1*$^{hypo/hypo}$ mice recapitulate the principal features of childhood long-segment HSCR and the early features of HAEC, including a failure to thrive, long-segment aganglionosis of the colon, the presence of hypertrophic cholinergic fibers in the distal colon, hyperplasia of goblet cells in the colon, mucus retention, a shift from acidic to neutral mucin production, crypt dilatation, and surface epithelial damage. Epithelial damage included focal epithelial necrosis and modest neutrophil infiltration, corresponding to mild cryptitis in human beings. Importantly, although the presence of most of these pathologic changes varied among the *Gfra1*$^{hypo/hypo}$ mouse colon samples at P4 and P10, 100% of the *Gfra1*$^{hypo/hypo}$ mice at both ages had a shift from acidic to neutral mucin production. By P10, 100% of *Gfra1*$^{hypo/hypo}$ mice also showed similar levels of goblet cell hyperplasia, whereas bacterial enterocyte adherence was not observed in any mice at this age. These results suggest that goblet cell dysfunction in the colon precedes the other pathologic changes, and that bacterial enterocyte adherence is not an initiating factor in HAEC. *Gfra1*$^{hypo/hypo}$ mice also provided us with an opportunity to study whether the observed altered goblet cell physiology results from the lack of the ENS in the colon and distal parts of the small intestine or developmental reduction in GFRa1 in the mesenchyme of the whole fetal intestine. We found that in the duodenum of *Gfra1*$^{hypo/hypo}$ mice both the goblet cell numbers and the mucin profile are normal, suggesting that colonic goblet cell hyperplasia results from the lack of ENS.

At a later age (P18–P25), all of the *Gfra1*$^{hypo/hypo}$ mice studied showed previously known features of HAEC, including copious mucus retention, epithelial damage in the colon, goblet cell hyperplasia mixed with goblet cell degeneration, and crypt dilatation and inflammation. Importantly, enterocyte adherence and bacterial invasion were present in only 2 of the 3 mice that had the most advanced epithelial damage, suggesting that enterocyte adherence and bacterial invasion are late events that mark the end stage of the disease. Taken together, our results suggest that HAEC may be associated with goblet cell dysfunction, which manifests first as a shift from acidic toward neutral mucin production in the early stage, followed by hyperplasia and a continuous mucin shift, and mucin overproduction during the later stages.[5] Over time, these features lead to mucus retention and crypt dilation, which in turn contribute to progressive dysfunction of the intestinal barrier, including progressive epithelial damage and ulceration; at the end stage of the disease, these pathologic changes facilitate bacterial enterocyte adherence, bacterial invasion, and, ultimately, sepsis.[6,7] Thus, our results shed light on the sequence of events in HAEC and suggest that addressing goblet cell dysplasia, which could remain in the proximal colon or transition zone after surgical removal of the aganglionic gut segment, may be beneficial in treating or preventing HAEC.

Together, mutations in endothelin-related genes that encode *EDN3*, *EDNRB*, and *ECE1* account for approximately

Figure 7. (***See previous page***). **Histopathologic analysis of moderate and marked HSCR/HAEC in P18–P25 *Gfra1*$^{hypo/hypo}$ mice.** (*A*–C) Exacerbated mucin type changes, epithelial damage, scarce inflammation in the lamina propria, and a lack of bacterial invasion in P18–P25 *Gfra1*$^{hypo/hypo}$ mice with moderate-grade HAEC. (*A*) In WT mice, the crypts in the colon (*A*1 and *A*2, *white arrow*) are relatively shallow and straight, and the surface epithelium is even and regularly palisading (*A*1, *curved black arrow*). The goblet cells in the surface epithelium and in the proximal parts of the crypts contain PAS-positive (ie, neutral) mucins, staining deep purple (*A*2, *white arrowhead*). In the basal parts of the crypts, apical mucin droplets in the colonocytes and the mucus in the goblet cells stain primarily with AB, staining light blue (mucin droplets; *A*2, *yellow arrowhead*) to dark blue (goblet cells; *A*2, *open arrowhead*). In *A*3, gram-positive (blue to black) and gram-negative (intense red) bacteria are isolated from the surface epithelium by a layer of mucus (*A*3, *black arrow*). (*B*) The intestinal lumens of *Gfra1*$^{hypo/hypo}$ mice contain fecal material and copious amounts of mucus with eosinophilic debris of shed epithelial cells (*B*1–*B*3, *white bold arrows*). The crypts were markedly dilated with retained mucin (*B*1–*B*3, *white arrow*). The surface epithelium had diffuse degeneration (*B*1 and *B*2, *curved black arrow*) and an increased number of goblet cells (*B*1–*B*3, *white arrowhead*). Multifocal necrotic and apoptotic colonocytes (*B*2 and *B*3, *open white arrowhead*) and scattered intraepithelial neutrophils (*B*2, *red open arrowhead*). (*C*) The basal lamina propria contains moderately increased numbers of eosinophils (*C*1, *black arrowhead*) and mildly increased numbers of lymphocytes (*C*1, *yellow open arrowhead*), indicative of an inflammatory process. Note the reduction in AB-stained (ie, acidic) mucin (*C*2, *black open arrowhead*) in the cytoplasm of basal crypt colonocytes. Gram staining shows copious amounts of mucus (*C*3, *black bold arrow*) and a lack of bacteria in mildly dilated crypts (*C*3, *white arrow*). (*D* and *E*) Marked epithelial damage at the surface epithelium, crypt abscesses, bacterial invasion, and inflammation in P18–P25 *Gfra1*$^{hypo/hypo}$ mice with marked HAEC score. (*D*) In *Gfra1*$^{hypo/hypo}$ mice, crypt dilatation (*D*1, *white arrow*) along with sparse neutrophil infiltrates in basal (*D*1, *red open arrowheads*) and apical (*D*2, *red open arrowheads*) crypt epithelium. The superficial epithelium shows multifocal necrotic areas and degenerative changes accompanied by superficial dense infiltrates of neutrophils (ie, microabscesses; *D*2, *green arrowheads*). Crypt abscesses (*E*1, *green arrow*), dense bacterial aggregates (*D*3, *black arrow*), and enterocyte-attaching bacteria (*D*3 and *E*2, *green bold arrow*) also are indicated. Bacteria inside a submucosal blood vessel (*E*3, *black arrow*) and a bacterial aggregate in mildly dilated crypt base (*E*3, *white arrow*) are present. Single granulocytes (*E*3, *yellow bold arrows*) and lymphocytes (*E*3, *yellow arrowheads*) are present in the lamina propria and submucosa, indicative of inflammation.

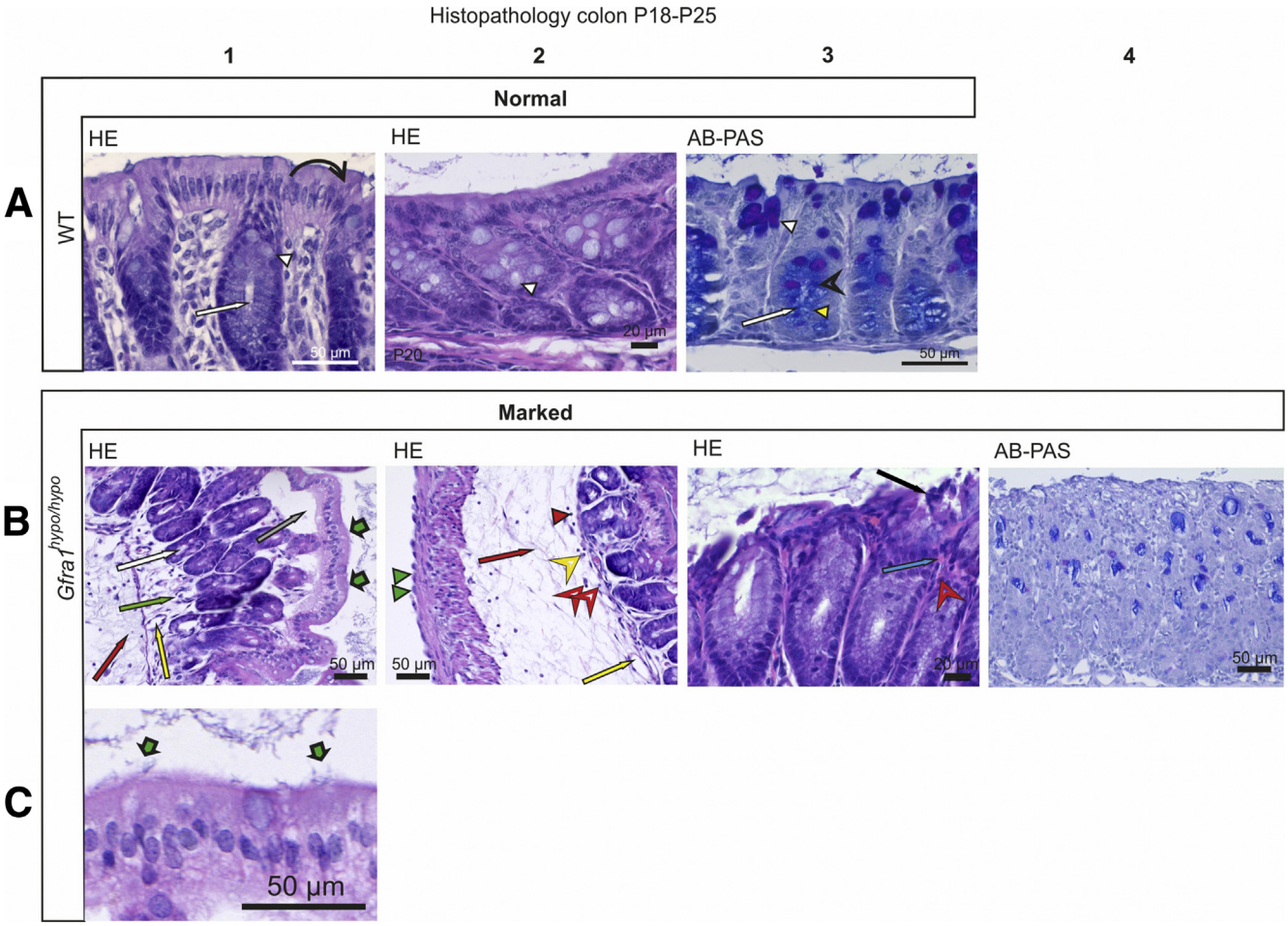

Figure 8. Histopathologic analysis of HSCR/HAEC in P18–P25 *Gfra1*$^{hypo/hypo}$ mice. (*A*) A WT colon. (*B* and *C*) Focal epithelial ulceration, variable colon wall changes after loss of mucosal integrity, and bacterial invasion in P18–P25 *Gfra1*$^{hypo/hypo}$ mice. Marked subepithelial edema (*B*1, *grey arrow*) and basal edema (*B*1, *green arrow*) in the lamina propria, and copious edema in the submucosa (*B*1, *red arrow*). Vacuole formation, indicative of acute degenerative changes (*B*1 and *B*2, *yellow arrow*) and mild dilatation of crypts in the colon (*B*1, *white arrow*) also are present. Copious numbers of bacteria are attached to the surface epithelium (*C*1, *green bold arrows*). Reactive mesothelial cells (*B*2, *green arrowheads*) and thin infiltrates of eosinophils (*B*2, *red arrowhead*), neutrophils (*B*2, *red open arrowheads*), and lymphocytes in the submucosa (*B*2, *yellow open arrowhead*) are present. Focal marked epithelial damage with epithelial degeneration and necrosis (*B*3, *black arrow*) are present. Subepithelial small hemorrhage (*B*3, *blue arrow*) and infiltrating neutrophils (*B*3, *red open arrowheads*) are present. Also evident is a relative absence of AB-PAS–positive cells (compare with panels *A*2 and *C*2 in Figure 7), which indicate goblet cell degeneration (*B*4).

5% of all HSCR cases.[1] Various animal models of HSCR with defective endothelin signaling have been generated, and substantial progress has been made using those models toward understanding short-segment HSCR and HAEC. A careful comparison between these endothelin-defective models and our *Gfra1*$^{hypo/hypo}$ mice is an important future objective. Such a study likely would show similarities—and probably also differences—between the 2 genotypes and might pave the way for the development of gene-specific treatment strategies.

To date, more than 10 HSCR susceptibility genes have been identified.[1,2,9,11,49] However, together these genes account for approximately 50% of all HSCR cases.[1,9,49] Thus, other genetic mutations and/or traits likely underlie HSCR. At present, neither GFRa1 protein nor *GFRa1* mRNA levels are routinely measured in colon samples resected from HSCR patients. One study using semiquantitative PCR reported reduced levels of *GFRa1* mRNA in 3 of 13 HSCR patients analyzed.[33] Given that our results show that reducing GFRa1 levels is sufficient to cause HSCR in mice, measuring *GFRa1* levels in a larger cohort of HSCR patients in conjunction with epigenetic and genomic sequencing analysis is an important future objective.

Materials and Methods

Animals

Gfra1^{hypo} mice (registered in the Mouse Genome Database as the 129Ola/ICR/C57BL6-Gfra1^{tm1Joao} mouse line) were generated by inserting a puΔtk cassette[31] into intron 6

Table 4. Summary of Histopathologic Findings at P18–P25

P18–P25	ID	Weight, *g*	Sex	Applied Teitelbaum et al[7] grade	Surface epithelial injury	Crypt dilation	Intraepithelial apoptotic remnants	Goblet cell hyperplasia	Mucins in crypts				Bacteria in crypts	Enterocyte adherence	Leukocytes	
									Mucin shift to PAS	Basal	Surface	Mucus retention			Granulocytes	Lymphocytes
WT	29.12.8-9	ND	ND	0	-	-	-	No	No	AB	PAS	-	-	No	-	-
WT	23.3-9-5	11.1	F	0	-	-	-	No	No	AB	PAS	-	-	No	-	-
WT	22.9.10CA-2	10.1	F	0	-	-	-	No	No	AB	PAS	-	-	No	-	-
WT	5.1.9-9	12.23	M	0	-	-	-	No	No	AB	PAS	-	-	No	-	-
WT/hypo	29.12.8-5	ND	ND	0	-	-	-	No	No	AB	PAS	-	-	No	-	+
WT/hypo	23.3-9-6	12.1	F	0	-	-	-	No	No	AB	PAS	-	-	No	-	-
WT/hypo	22.9.10CA-7	84	F	0	-	-	-	No	No	AB	PAS	-	-	No	-	-
WT/hypo	22.9.10 CA-8	8.9	F	0	-	-	-	No	No	AB	PAS	-	-	No	-	-
Hypo/hypo	29.12.8-8	ND	ND	III/IV	Marked	++	++	Degenerated	Yes	PAS	AB	+	+	Yes	++	-
Hypo/hypo	23.3-9-4	9.4	M	II	Moderate	++	+	Yes	Yes	PAS/foamy AB	PAS/foamy AB	++	-	No	-	+
Hypo/hypo	22.9.10CA-3	8.5	M	III/IV	Marked	+/++	++	Yes + degenerated	Degenerated	degenerated	Atypical AB	+	-	No	++	+
Hypo/hypo	22.9.10 CA-10	7.8	F	II	Moderate	++/+++	++	Yes	Yes	PAS/foamy AB	PAS/foamy AB	++	-	No	+	+
Hypo/hypo	5.1.9-7	8.8	M	IV/V	Marked	++/+++	+++	Yes + degenerated	Yes	PAS/foamy AB	PAS/foamy AB	+/++	++	Yes	+	+
					Minimal	Mild +	Mild +					Mild +	Mild +		Normal - (<4/HPF)	
				0–V	Mild	Moderate ++	Moderate ++	Yes/no	Yes/no			Moderate ++	Moderate ++	Yes/no	Mild + (5–15/HPF)	
					Moderate	Marked +++	Marked +++					Marked +++			Moderate ++ (20–30/HPF)	
					Marked											

NOTE. See the Materials and Methods section for details regarding histopathologic grading.
ND, not determined.

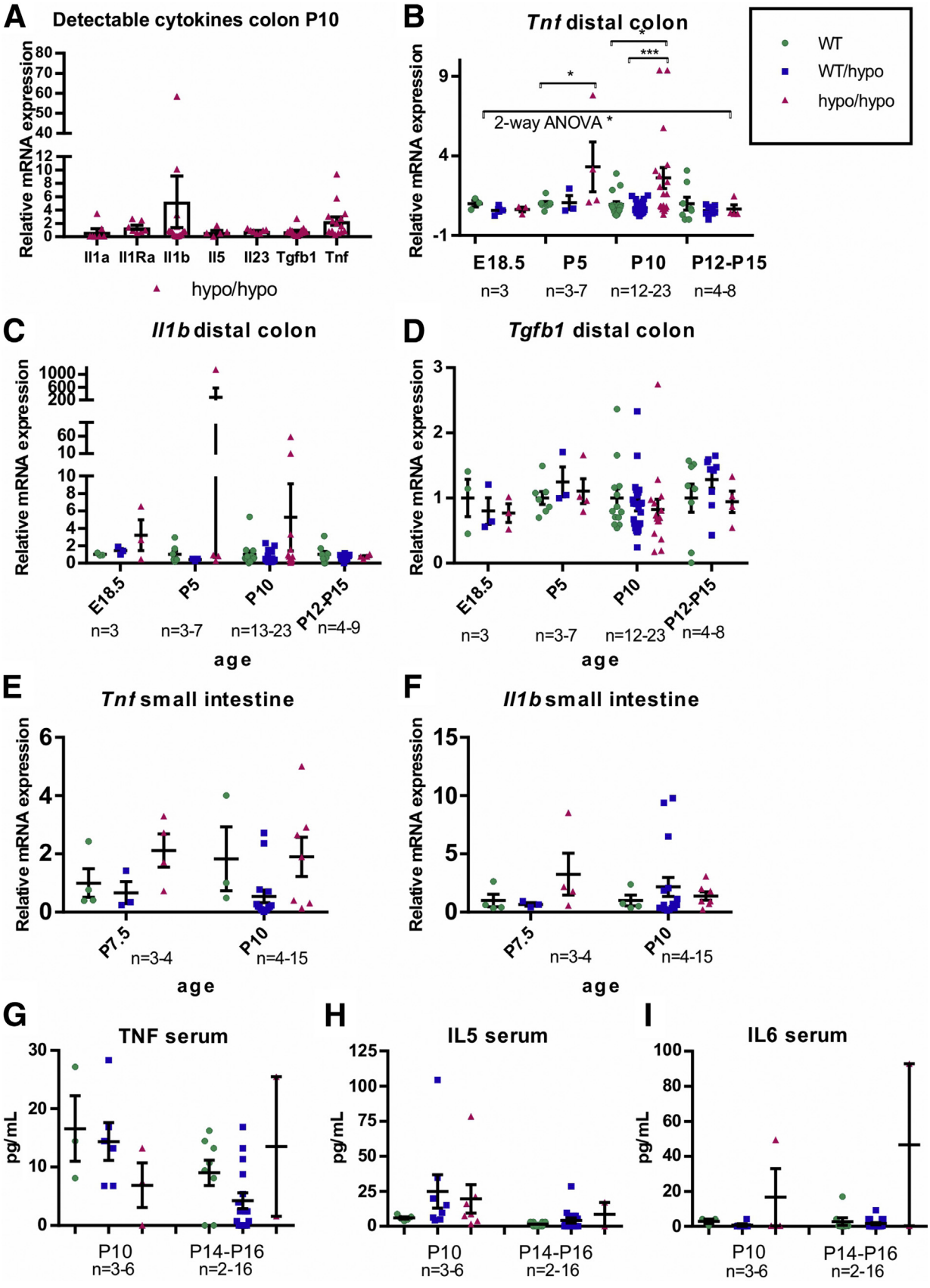
A
Detectable cytokines colon P10
Relative mRNA expression
Il1a Il1Ra Il1b Il5 Il23 Tgfb1 Tnf
hypo/hypo
B
Tnf distal colon
Relative mRNA expression
2-way ANOVA *
E18.5 P5 P10 P12-P15
n=3 n=3-7 n=12-23 n=4-8
WT
WT/hypo
hypo/hypo
C
Il1b distal colon
Relative mRNA expression
E18.5 P5 P10 P12-P15
n=3 n=3-7 n=13-23 n=4-9
age
D
Tgfb1 distal colon
Relative mRNA expression
E18.5 P5 P10 P12-P15
n=3 n=3-7 n=12-23 n=4-8
age
E
Tnf small intestine
Relative mRNA expression
P7.5 P10
n=3-4 n=4-15
age
F
Il1b small intestine
Relative mRNA expression
P7.5 P10
n=3-4 n=4-15
age
G
TNF serum
pg/mL
P10 P14-P16
n=3-6 n=2-16
H
IL5 serum
pg/mL
P10 P14-P16
n=3-6 n=2-16
I
IL6 serum
pg/mL
P10 P14-P16
n=3-6 n=2-16

of the *Gfra1* gene using gene targeting via homologous recombination in embryonic stem cells (Figure 1*A*–*C*). Embryonic stem cell clones that had undergone homologous recombination in 1 *Gfra1* allele were identified by performing Southern blot analysis on *Eco*RV-digested genomic DNA using the probe indicated in Figure 1*A* (expected sizes: targeted, 7564 bp; WT, 10397 bp). Routine PCR-based genotyping of the offspring was performed using the primers indicated in Figure 1*A* (GfraloxF forward: 5'-cattggccaggtgaaagaca; Gfra1loxR reverse: 5'-agaaagaga gatgatcacagtacacatg). The mice were maintained on a 129Ola/ICR/C57BL6 mixed genetic background, housed under a 12-hour/12-hour light/dark cycle at 20°C–22°C, with 1 mother and litter per cage; standard chow and water were available ad libitum. All animal experiments were approved by the National Animal Experiment Board of Finland.

Tissue Processing

Paraffin-embedded sections, whole-mount GI tracts (E13.5), and myenteric plexuses (P10 or P18–P25) were used for histologic preparations. Comparable samples obtained from the duodenum, ileum, and colon were analyzed from all genotypes, using littermates as controls. The samples were fixed in 4% paraformaldehyde in phosphate-buffered saline (PBS) for 24 hours at room temperature. Automated dehydration of the tissues and subsequent paraffin embedding were performed using an ASP300 S tissue processor (Leica, Wetzlar, Germany). Paraffin blocks were cut to prepare 5-μm sections using a Tissue-Tek microtome (Sakura, Alphen aan den Rijn, The Netherlands). For whole-mount histology of P10 and P18–P25 tissues, the mice were perfused intracardially with PBS and 4% paraformaldehyde. The longitudinal muscle/myenteric plexus (LMMP) preparations were isolated under a dissection microscope by peeling off the outer muscle layer of the GI tract and postfixed for 15 minutes in paraformaldehyde.

Histopathology

Paraffin sections of the duodenum and colon were stained with H&E, Gram stain, or a combination of AB (pH 2.5) and PAS using standard protocols. LMMPs from the small and large intestine were stained for acetylcholinesterase as previously described.[50] Briefly, LMMP was washed in PBS for 1 hour, 100 mmol/L maleic acid buffer pH 6.0 for 5 minutes, pre-incubated for 30 minutes in 65 mmol/L maleic acid buffer including 0.5 mol/L potassium ferricyanide, 4 mmol/L copper sulfate, and 5 mmol/L sodium citrate, and reacted for 30–45 minutes in 5 mmol/L acetylthiocholine iodide in 100 mmol/L maleic acid buffer. NADPH diaphorase was used to visualize nitrergic neurons in LMMPs; briefly, LMMPs were washed 2 times 1 hour in PBS and reacted 1 hour at +37°C in a solution prepared right before use containing 0.3% Triton (Sigma) X-100, 0.01% nitro blue tetrazolium chloride, and 0.1% NADPH in PBS. Finally, the LMMP preparations were washed 6 times for 5 minutes in PBS and mounted in glycerol for imaging.

Histopathology Grading

The criteria for histopathologic grading are defined later. HAEC-associated inflammatory cell infiltration of the crypts (cryptitis and crypt abscesses) was milder in mice than in human beings, whereas epithelial pathology characteristic of HAEC was recapitulated well in mice. Therefore, we modified the grading system reported by Teitelbaum et al[7] to primarily reflect epithelial pathology.

Surface epithelial damage. Epithelial damage was graded as minimal, mild, moderate, or marked.

Minimal surface epithelial damage. The surface epithelium consists of mild disorganization and slight degeneration of the surface epithelium. In contrast to regular palisading, colonocytes are clustered multifocally in disorganized, undulating rows with partially overlapping nuclei. Apical eosinophilia and indistinct cell borders are also visible focally.

Mild surface epithelial damage. The surface epithelium has mild to moderate disorganization and mild degenerative changes. The size and shape of the epithelial cells and nuclei vary, and they grow in disorganized, undulating rows with partially overlapping nuclei. Apical cytoplasms are generally homogenously eosinophilic or vacuolar, and the cell borders are indistinct; cells are occasionally low columnar to cuboidal in shape. Scattered intraepithelial apoptotic/necrotic cell remnants are present.

Moderate surface epithelial damage. The lumen of the intestine contains copious amounts of mucus and deeply eosinophilic debris of shed epithelial cells. The surface epithelium has multifocal to diffuse moderate degeneration and cuboidal to flattened cells with indistinct cell borders and intense staining. Increased numbers of apoptotic/necrotic cells or cell remnants are present, as well as clusters of apoptotic/necrotic cells. Scattered intraepithelial neutrophils (1–5 per high-power field [HPF]) may be present in the lamina propria. Mildly increased numbers of lymphocytes in the basal lamina propria (indicative of mild chronic colitis) were detected in 1 mouse; however, in accordance with a previous report on HAEC in mice,[44] inflammatory activity is generally very low.

Marked surface epithelial damage. The surface epithelium has generally diffuse degeneration, and multiple

Figure 9. (***See previous page***). **Analysis of cytokine mRNA and protein levels.** (*A*–*D*) qPCR analysis of cytokine mRNA levels in the colon of *Gfra1*$^{hypo/hypo}$ and control mice at indicated ages. *Tnf* mRNA levels are up-regulated in P5 colon ($P < .05$, analysis of variance and Tukey multiple comparisons) and in P10 colon ($P < .05$, analysis of variance and Tukey multiple comparisons). (*E* and *F*) *Tnf* and *Il1b* mRNA levels are not up-regulated in the small intestine (a segment spanning the duodenum–jejunum was analyzed). (*G*–*I*) Measurements of serum cytokine protein levels by ELISA. In analysis of *Gfra1*$^{hypo/hypo}$ and control mice at the indicated ages, no significant differences between the genotypes were observed. The number of animals is given for each time point in the Figure panels (qPCR: 2–3 biological replicates, 1–2 independent experiments per animal; ELISA: 2 biological replicates, 1 experiment per animal). All summary data are presented as means ± SEM. *$P < .05$, **$P < .01$, and ***$P < .001$.

necrotic areas accompanied by small superficial infiltrates of neutrophils (microabscesses) are present. The apical parts of the crypts of Lieberkühn contain few to several intraepithelial neutrophils with sporadic crypt abscesses. The goblet cells are degenerated. The lamina propria contains mildly to moderately increased numbers of eosinophils and neutrophils in the basal areas and between the crypts. The inflammatory reaction in the intestinal wall is mild.

Loss of integrity of the gut wall/bacterial invasion. The surface epithelium shows gross changes of varying degrees. The lamina propria has mild to moderate edema and mildly to moderately increased numbers of eosinophils, neutrophils, and lymphocytes. Profuse bacterial accumulates are present in some of the moderately to markedly dilated crypts of Lieberkühn. The submucosa has marked edema, sparse infiltrates of leukocytes, and small numbers of bacteria. The circular and longitudinal muscle layers have marked diffuse degeneration and moderate neutrophilic infiltrates. Mesothelial cells are reactive.

Crypt dilatation. Crypt dilatation was graded as minimal to mild (+), moderate (++), or marked (+++) to quantify the extent of the changes. In cases in which large segmental variation was present, both grades were reported.

Mild crypt dilatation. The dilatation is present primarily at the base of the crypts, and any from a few to approximately half of the crypts are affected.

Moderate crypt dilatation. Most of the crypts are affected.

Marked crypt dilatation. The apical areas of the crypts also are affected, and most of the crypts are affected.

Leukocyte numbers in the mucosa. A 3-tier system was used to grade leukocyte numbers as minimal to mild (+), moderate (++), and marked (+++).

Lymphocytes. Lymphocyte number is considered to be normal if 5 or fewer cells are generally present in the lamina propria between the crypts per HPF. A minimal to mild increase in lymphocytes is scored if they fill the intercryptal region, and they may be increased basally below the crypt bases. There is no increase in separation of the crypts. A moderate increase is scored if the lymphocytes increase the separation of the crypts; a marked increase is scored if there is a diffuse distribution of lymphocytes with distortion of the cryptal architecture. In accordance with a previous report of HAEC in mice,[44] none of our samples contained moderate or marked increases in lymphocytes. Accordingly, extremely few plasma cells were detected, and plasma cells therefore were excluded from grading.

Granulocytes. Eosinophils and neutrophils were graded as a single entity. Neutrophils related to surface epithelial damage (eg, crypt abscesses, microabscesses in the epithelium, and epithelial neutrophils) were omitted from this section and were graded under surface epithelial damage.

Granulocyte number is considered to be normal if no more than 3–4 granulocytes typically are present per HPF in the lamina propria. A minimal to mild increase is scored if approximately 15 granulocytes are present per HPF in the lamina propria. A moderate increase is scored if the infiltrate contains 20–30 granulocytes per HPF; this may be accompanied by macrophages. A marked increase is scored if granulocytes are the dominant population and are not easily counted per HPF.

Quantification of Goblet Cells

Goblet cells were counted in the distal third of the colon from the basal half of the crypts. Twenty to 30 crypts were counted per sample. Goblet cells that primarily were stained light blue were counted as AB+ and goblet cells stained primarily magenta or purple were counted as PAS+. Goblet cells fitting neither category were counted as AB-PAS+. Sample genotypes were blinded for the counter.

Immunohistochemistry

Sections were deparaffinized through serial washes with xylene, alcohol, and water. Antigen retrieval was performed by boiling the samples for 10 minutes in citrate buffer (10 mmol/L sodium citrate, 0.05% Tween 20, pH 6.0). Endogenous peroxidase activity was quenched in 1:53 H_2O_2 standard solution in Tris-buffered saline (TBS) for 30 minutes at room temperature. After washing with TBS containing 0.1% Tween 20, the tissue was blocked in 1.5% normal goat serum in TBS containing 0.1% Tween 20 for 30 minutes at room temperature. The sections were incubated overnight at 4°C in primary antibody solution containing rabbit anti-ubiquitin C-terminal hydrolase L1 (1:250, BML-PG9500; Enzo Life Sciences) or rabbit anti–glial fibrillary acidic protein (1:200, Ab-4 RB-087-A; ThermoScientific). After washing, the sections were incubated for 90 minutes at room temperature in secondary antibody solution containing biotinylated anti-rabbit antibody (1:200; Vector Laboratories) or goat anti-rabbit Alexa 488 antibody (1:400, A11034; Invitrogen). The biotinylated secondary antibody signal was enhanced using the ABC reaction kit (PK-4001, Vector Laboratories) and visualized using 3,3′-diaminobenzidine (SK-4100, Vector Laboratories). Samples were dehydrated through serial washes with water, alcohol, and xylene, and mounted using Depex (Science Services GmbH, München, Germany). Fluorescence-labeled, whole-mount samples were mounted in glycerol and imaged using an Olympus BX-61 microscope. As negative controls, either the primary or secondary antibody was omitted.

ELISA

ELISA was performed with commercial kits according to the manufacturer's instructions (Invitrogen ProcartaPlex multiplex interferon γ, IL12, IL4, IL5, IL6, TNF, EPX060-20831-90, IL1B Mouse ProcartaPlex Simplex Kit, EPX01A-26002-901, and IL9 Mouse ProcartaPlex Simplex Kit, EPX01A-26041-901).

Quantitative PCR

RNA isolation. RNA was isolated from snap-frozen tissues using the TRIzol reagent (Invitrogen) for samples collected from E18.5 on or the RNAqueous Micro-kit (AM1931; Life Technologies) in accordance with the manufacturer's instructions. DNase I was supplied in the same kit.

Reverse transcription. First-strand complementary DNA (cDNA) was synthesized from 50 to 300 ng of RNA (with

equal amounts of starting RNA used in each experiment) using random hexamer primers in a final volume of 20 μL (Transcriptor First-Strand cDNA synthesis kit; Roche). In brief, 2 μL of random hexamer primers was mixed with 11 μL of RNA sample diluted in nuclease-free water and incubated at 65°C for 10 minutes. Next, 7 μL of a mixture containing 4 μL of 5× reverse transcriptase buffer, 2 μL of 100 mmol/L deoxynucleoside triphosphate, 0.5 μL of RNase inhibitor, and 0.5 μL of Transcriptor reverse transcriptase (Transcriptor First-Strand cDNA synthesis kit; Roche) were added, mixed gently, and incubated at 25°C for 10 minutes, 55°C for 30 minutes, and 85°C for 5 minutes. A control sample containing no reverse transcriptase was included in each experiment. The cDNA was cooled on ice, diluted 1:15 in water, and either stored at -20°C or used immediately for quantitative PCR (qPCR).

Real-time qPCR. qPCR was performed using the LightCycler 480 real-time PCR system (Roche Diagnostics) with the LightCycler 480 SYBR Green I Master mix and 2.5 pmol of primers at a final volume of 10 μL. The reactions were run on white 384-well plates sealed with adhesive plate sealers (04729749001; Roche Diagnostics). Each reaction contained 2.5 μL of diluted cDNA. Each qPCR run contained 2–3 replicates of each reaction. The following qPCR program was used: pre-incubation: 10 minutes at 95°C; amplification: 10 seconds at 95°C, 15 seconds at 60°C, and 15 seconds at 72°C for 45 cycles; melting curve: 5 seconds at 95°C, 30 seconds at 55°C, continuous acquisition mode at 95°C with 2 acquisitions per degree Celsius; and cooling: 10 seconds at 40°C. The data were analyzed using LightCycler 480 Software Release 1.5.0 SP1, with the Absolute Quantification/2nd Derivative Max calculation. *Actb* was amplified as a reference gene. The following *mus musculus* (m) primer sets were used in this study: m*Actb*: 5′-ctaaggccaaccgtgaaaag and 5′-accagaggcatacagggaca; m*Gdnf* ex2–3: 5′-cgctgaccagt gactccaatatgc and 5′-tgccgcttgtttatctggtgacc; m*Gfra1*: 5′-ttcc cacacacgttttacca and 5′-gcccgatacattggatttca; m*Ifng*: 5′-ttctt cagcaacagcaaggc and 5′-tcagcagcgactccttttcc; m*Il1b*: 5′-agttga cggaccccaaaag and 5′-agctggatgctctcatcagg; m*Il1a*: 5′-gtcgg caaagaaatcaagatg and 5′-gtcttcgttttcactgtaacag; m*Il1Ra*: 5′-aa ccagctcattgctgggtactta and 5′-gcccaagaacacactatgaaggtc; m*Il2*: 5′-ttgtgctccttgtcaacagc and 5′-ctggggagtttcaggttcct; m*Il4*: 5′-aa cgaggtcacaggagaagg and 5′-tctgcagctccatgagaaca; m*Il5*: 5′-ac cgagctctgttgacaag and 5′-tcctcgccacacttctcttt; m*Il6*: 5′-accac ttcacaagtcggagg and 5′-tgcaagtgcatcatcgttgt; m*Il10*: 5′-ataact gcacccacttccca and 5′-cttggcaacccaagtaaccc; m*Il13*: 5′-gca gcatggtatggagtgtg and 5′-tggcgaaacagttgctttgt; m*Il23*: 5′-gctgt gcctaggagtagcag and 5′-tggctgttgtccttgagtcc; m*Ret* t2 : 5′-tccc ttccacatggattga and 5′-atcggctctcgtgagtggta; m*Tgfb1*: 5′-tgga gcaacatgtggaactc and 5′-gtcagcagccggttacca; and m*Tnf*: 5′-gatc ggtccccaaagggatg and 5′-tgagggtctgggccatagaa.

Western Blot Analysis

Snap-frozen E12.5 tissue was homogenized in a homogenization solution containing 0.3 mol/L sucrose, 10 mmol/L HEPES, 1 mmol/L EDTA (pH 7.2–7.4), and a proteinase inhibitor (Complete Mini-Tabs Cocktail Set; Roche); the protein concentration was measured using the Lowry method (Bio-Rad). A total of 5–10 μg of protein was mixed with Laemmli sample buffer and incubated at 95°C for 5 minutes. The proteins were separated on an 8% sodium dodecyl sulfate–polyacrylamide gel electrophoresis and transferred to a nitrocellulose membrane (Amersham Protran, GE Healthcare). After washing and blocking at room temperature for 60 minutes in 5% milk, the membranes were incubated in goat anti-Gfra1 antibody (1:1000, GT15004; Neuromics). After washing, the membranes were incubated at room temperature for 2 hours in horseradish peroxidase–conjugated anti-goat antibody (1:2000, P0449; Dako). The protein bands were visualized using enhanced chemiluminescence substrate (Pierce). As a loading control, the membranes then were stripped and reprobed using anti–α-tubulin antibody (1:60,000, T9026; Sigma), followed by horseradish peroxidase–conjugated donkey anti-mouse antibody (1:2000, P0449; Dako). Three independent Western blots were quantified with ImageJ 1.50a software (National Institutes of Health, Bethesda, MD) and an unpaired Student *t* test was performed as a statistical analysis using GraphPad Prism software.

Luciferase Assay

RET-dependent activation of mitogen-activated protein kinase by soluble GFRa1 was measured using MG87 fibroblasts that stably express RET (MG87RET) and the PathDetect-Elk1 system (219005; Stratagene). One day before the assay, cells were plated in a 96-well plate (20,000 cells/well) in 100 μL/well Dulbecco's modified Eagle medium containing 10% fetal bovine serum and 100 μg/mL normocin (ant-nr-1; InvivoGEN) and cultured overnight in an incubator with 5% CO_2. Soluble GFRa1 (1–5000 ng/mL, 560-GR; R&D Systems) and GDNF (100 ng/mL 450-10; Peprotech) were added to wells in quadruplicate per GFRa1 concentration. The plates then were cultured for an additional 22–24 hours for luciferase expression, after which the culture media was discarded and the cells were incubated with NeoLite reagent (6016711; Perkin Elmer) for 10 minutes. Luciferase activity was measured using a MicroBeta 2 (PerkinElmer) plate counter. Each experiment was performed twice, and the results were analyzed using GraphPad Prism software.

References

1. Amiel J, Sproat-Emison E, Garcia-Barcelo M, Lantieri F, Burzynski G, Borrego S, Pelet A, Arnold S, Miao X, Griseri P, Brooks AS, Antinolo G, de Pontual L, Clement-Ziza M, Munnich A, Kashuk C, West K, Wong KK, Lyonnet S, Chakravarti A, Tam PK, Ceccherini I, Hofstra RM, Fernandez R, Hirschsprung Disease C. Hirschsprung disease, associated syndromes and genetics: a review. J Med Genet 2008;45:1–14.
2. Butler Tjaden NE, Trainor PA. The developmental etiology and pathogenesis of Hirschsprung disease. Transl Res 2013;162:1–15.
3. Lister J, Tam PKH. Hirschsprung's disease. In: Lister J, Irving IM, eds. Neonatal surgery. London: Butterworth, 1990:523–546.

4. Frykman PK, Short SS. Hirschsprung-associated enterocolitis: prevention and therapy. Semin Pediatr Surg 2012;21:328–335.
5. Murphy F, Puri P. New insights into the pathogenesis of Hirschsprung's associated enterocolitis. Pediatr Surg Int 2005;21:773–779.
6. Demehri FR, Halaweish IF, Coran AG, Teitelbaum DH. Hirschsprung-associated enterocolitis: pathogenesis, treatment and prevention. Pediatr Surg Int 2013; 29:873–881.
7. Teitelbaum DH, Caniano DA, Qualman SJ. The pathophysiology of Hirschsprung's-associated enterocolitis: importance of histologic correlates. J Pediatr Surg 1989; 24:1271–1277.
8. Burzynski GM, Nolte IM, Bronda A, Bos KK, Osinga J, Plaza Menacho I, Twigt B, Maas S, Brooks AS, Verheij JB, Buys CH, Hofstra RM. Identifying candidate Hirschsprung disease-associated RET variants. Am J Human Genet 2005;76:850–858.
9. Goldstein AM, Hofstra RM, Burns AJ. Building a brain in the gut: development of the enteric nervous system. Clin Genet 2013;83:307–316.
10. Kenny SE, Tam PK, Garcia-Barcelo M. Hirschsprung's disease. Semin Pediatr Surg 2010;19:194–200.
11. Plaza-Menacho I, Burzynski GM, de Groot JW, Eggen BJ, Hofstra RM. Current concepts in RET-related genetics, signaling and therapeutics. Trends Genet 2006; 22:627–636.
12. Jiang Q, Ho YY, Hao L, Nichols Berrios C, Chakravarti A. Copy number variants in candidate genes are genetic modifiers of Hirschsprung disease. PLoS One 2011; 6:e21219.
13. Wallace AS, Anderson RB. Genetic interactions and modifier genes in Hirschsprung's disease. World J Gastroenterol 2011;17:4937–4944.
14. Airaksinen MS, Saarma M. The GDNF family: signalling, biological functions and therapeutic value. Nat Rev Neurosci 2002;3:383–394.
15. Sasselli V, Pachnis V, Burns AJ. The enteric nervous system. Dev Biol 2012;366:64–73.
16. Young HM, Hearn CJ, Ciampoli D, Southwell BR, Brunet JF, Newgreen DF. A single rostrocaudal colonization of the rodent intestine by enteric neuron precursors is revealed by the expression of Phox2b, Ret, and p75 and by explants grown under the kidney capsule or in organ culture. Dev Biol 1998; 202:67–84.
17. Heanue TA, Pachnis V. Enteric nervous system development and Hirschsprung's disease: advances in genetic and stem cell studies. Nat Rev Neurosci 2007;8:466–479.
18. Uesaka T, Nagashimada M, Yonemura S, Enomoto H. Diminished Ret expression compromises neuronal survival in the colon and causes intestinal aganglionosis in mice. J Clin Invest 2008;118:1890–1898.
19. Uesaka T, Nagashimada M, Enomoto H. GDNF signaling levels control migration and neuronal differentiation of enteric ganglion precursors. J Neurosci 2013; 33:16372–16382.
20. Enomoto H, Araki T, Jackman A, Heuckeroth RO, Snider WD, Johnson EM Jr, Milbrandt J. GFR alpha1-deficient mice have deficits in the enteric nervous system and kidneys. Neuron 1998;21:317–324.
21. Pichel JG, Shen L, Sheng HZ, Granholm AC, Drago J, Grinberg A, Lee EJ, Huang SP, Saarma M, Hoffer BJ, Sariola H, Westphal H. Defects in enteric innervation and kidney development in mice lacking GDNF. Nature 1996; 382:73–76.
22. Schuchardt A, D'Agati V, Larsson-Blomberg L, Costantini F, Pachnis V. Defects in the kidney and enteric nervous system of mice lacking the tyrosine kinase receptor Ret. Nature 1994;367:380–383.
23. Gianino S, Grider JR, Cresswell J, Enomoto H, Heuckeroth RO. GDNF availability determines enteric neuron number by controlling precursor proliferation. Development 2003;130:2187–2198.
24. de Graaff E, Srinivas S, Kilkenny C, D'Agati V, Mankoo BS, Costantini F, Pachnis V. Differential activities of the RET tyrosine kinase receptor isoforms during mammalian embryogenesis. Genes Dev 2001; 15:2433–2444.
25. Uesaka T, Jain S, Yonemura S, Uchiyama Y, Milbrandt J, Enomoto H. Conditional ablation of GFRalpha1 in postmigratory enteric neurons triggers unconventional neuronal death in the colon and causes a Hirschsprung's disease phenotype. Development 2007;134:2171–2181.
26. Wu L, Gu J, Cui H, Zhang QY, Behr M, Fang C, Weng Y, Kluetzman K, Swiatek PJ, Yang W, Kaminsky L, Ding X. Transgenic mice with a hypomorphic NADPH-cytochrome P450 reductase gene: effects on development, reproduction, and microsomal cytochrome P450. J Pharmacol Exp Ther 2005;312:35–43.
27. Meyers EN, Lewandoski M, Martin GR. An Fgf8 mutant allelic series generated by Cre- and Flp-mediated recombination. Nat Genet 1998;18:136–141.
28. Nagy A, Moens C, Ivanyi E, Pawling J, Gertsenstein M, Hadjantonakis AK, Pirity M, Rossant J. Dissecting the role of N-myc in development using a single targeting vector to generate a series of alleles. Curr Biol 1998; 8:661–664.
29. Wei Y, Zhou X, Fang C, Li L, Kluetzman K, Yang W, Zhang QY, Ding X. Generation of a mouse model with a reversible hypomorphic cytochrome P450 reductase gene: utility for tissue-specific rescue of the reductase expression, and insights from a resultant mouse model with global suppression of P450 reductase expression in extrahepatic tissues. J Pharmacol Exp Ther 2010; 334:69–77.
30. Wang B, He L, Dong H, Dalton TP, Nebert DW. Generation of a Slc39a8 hypomorph mouse: markedly decreased ZIP8 Zn(2)(+)/(HCO(3)(-))(2) transporter expression. Biochem Biophys Res Commun 2011; 410:289–294.
31. Chen YT, Bradley A. A new positive/negative selectable marker, puDeltatk, for use in embryonic stem cells. Genesis 2000;28:31–35.
32. Durbec PL, Larsson-Blomberg LB, Schuchardt A, Costantini F, Pachnis V. Common origin and developmental dependence on c-ret of subsets of enteric and sympathetic neuroblasts. Development 1996; 122:349–358.

33. Lui VC, Samy ET, Sham MH, Mulligan LM, Tam PK. Glial cell line-derived neurotrophic factor family receptors are abnormally expressed in aganglionic bowel of a subpopulation of patients with Hirschsprung's disease. Lab Invest 2002;82:703–712.
34. Worley DS, Pisano JM, Choi ED, Walus L, Hession CA, Cate RL, Sanicola M, Birren SJ. Developmental regulation of GDNF response and receptor expression in the enteric nervous system. Development 2000; 127:4383–4393.
35. Cacalano G, Farinas I, Wang LC, Hagler K, Forgie A, Moore M, Armanini M, Phillips H, Ryan AM, Reichardt LF, Hynes M, Davies A, Rosenthal A. GFRalpha1 is an essential receptor component for GDNF in the developing nervous system and kidney. Neuron 1998;21:53–62.
36. Sidorova YA, Matlik K, Paveliev M, Lindahl M, Piranen E, Milbrandt J, Arumae U, Saarma M, Bespalov MM. Persephin signaling through GFRalpha1: the potential for the treatment of Parkinson's disease. Mol Cell Neurosci 2010;44:223–232.
37. Ryan ET, Ecker JL, Christakis NA, Folkman J. Hirschsprung's disease: associated abnormalities and demography. J Pediatr Surg 1992;27:76–81.
38. Payette RF, Tennyson VM, Pham TD, Mawe GM, Pomeranz HD, Rothman TP, Gershon MD. Origin and morphology of nerve fibers in the aganglionic colon of the lethal spotted (ls/ls) mutant mouse. J Comp Neurol 1987;257:237–252.
39. Tam PK, Boyd GP. Origin, course, and endings of abnormal enteric nerve fibres in Hirschsprung's disease defined by whole-mount immunohistochemistry. J Pediatr Surg 1990;25:457–461.
40. Niemi M, Kouvalainen K, Hjelt L. Cholinesterases and monoamine oxidase in congenital megacolon. J Pathol Bacteriol 1961;82:363–366.
41. Kamijo K, Hiatt RB, Koelle GB. Congenital megacolon; a comparison of the spastic and hypertrophied segments with respect to cholinesterase activities and sensitivities to acetylcholine, DFP and the barium ion. Gastroenterology 1953;24:173–185.
42. Bealer JF, Natuzzi ES, Buscher C, Ursell PC, Flake AW, Adzick NS, Harrison MR. Nitric oxide synthase is deficient in the aganglionic colon of patients with Hirschsprung's disease. Pediatrics 1994;93:647–651.
43. Vanderwinden JM, De Laet MH, Schiffmann SN, Mailleux P, Lowenstein CJ, Snyder SH, Vanderhaeghen JJ. Nitric oxide synthase distribution in the enteric nervous system of Hirschsprung's disease. Gastroenterology 1993;105:969–973.
44. Cheng Z, Dhall D, Zhao L, Wang HL, Doherty TM, Bresee C, Frykman PK. Murine model of Hirschsprung-associated enterocolitis. I: phenotypic characterization with development of a histopathologic grading system. J Pediatr Surg 2010;45:475–482.
45. Pelaseyed T, Bergstrom JH, Gustafsson JK, Ermund A, Birchenough GM, Schutte A, van der Post S, Svensson F, Rodriguez-Pineiro AM, Nystrom EE, Wising C, Johansson ME, Hansson GC. The mucus and mucins of the goblet cells and enterocytes provide the first defense line of the gastrointestinal tract and interact with the immune system. Immunol Rev 2014;260:8–20.
46. Thiagarajah JR, Yildiz H, Carlson T, Thomas AR, Steiger C, Pieretti A, Zukerberg LR, Carrier RL, Goldstein AM. Altered goblet cell differentiation and surface mucus properties in Hirschsprung disease. PLoS One 2014;9:e99944.
47. Nakamura H, Tomuschat C, Coyle D, O'Donnel A-M, Lim T, Puri P. Altered goblet cell function in Hirschsprung's disease. Pediatr Surg Int 2018;34:121–128.
48. Ledda F, Paratcha G, Sandoval-Guzman T, Ibanez CF. GDNF and GFRalpha1 promote formation of neuronal synapses by ligand-induced cell adhesion. Nat Neurosci 2007;10:293–300.
49. Kapur RP. Practical pathology and genetics of Hirschsprung's disease. Semin Pediatr Surg 2009; 18:212–223.
50. Vincent SR. Histochemistry of endogenous enzymes. In: Bolam JP, ed. Experimental neuroanatomy: a practical approach. Oxford: IRL Press, 1992:154–155.

Received July 1, 2016. Accepted December 19, 2018.

Correspondence
Address correspondence to: Jaan-Olle Andressoo, PhD, Department of Pharmacology, Faculty of Medicine, Helsinki Institute of Life Science, University of Helsinki, PO Box 63, 00014 Helsinki, Finland. e-mail: jaan-olle.andressoo@helsinki.fi.

Acknowledgments
L. Lauriina Porokuokka and Heikki T. Virtanen are currently affiliated with the Department of Pharmacology, Faculty of Medicine & Helsinki Institute of Life Science, University of Helsinki, Helsinki, Finland, P.O. Box 63, 00014 Helsinki, Finland.

Jaan-Olle Andressoo is currently affiliated with the Department of Pharmacology, Faculty of Medicine & Helsinki Institute of Life Science, University of Helsinki, Helsinki, Finland, P.O. Box 63, 00014 Helsinki, Finland and Division of Neurogeriatrics, Department of Neurobiology, Care Sciences and Society, Karolinska Institutet SE-171 77 Stockholm, Sweden.

The authors would like to thank Ms Susanne Dahlström, Ms Jenni Montonen, and personnel of the Finnish Centre for Laboratory Animal Pathology for help with experimental procedures, Ms Ana Montaño-Rodríguez and Ms Sonja Huovila for help with the artwork, and Mr Mark C. Cowlishaw for English language editing.

Author contributions
L. Lauriina Porokuokka acquired, analyzed, and interpreted the data, drafted the manuscript, and performed the statistical analysis; Heikki T. Virtanen acquired, analyzed, and interpreted the data; Jere Linden acquired, analyzed, and interpreted the histopathologic data and drafted the manuscript; Yulia A. Sidorova acquired, analyzed, and interpreted the data and drafted the manuscript; Tatiana Danilova acquired, analyzed, and interpreted the data; Maria Lindahl analyzed and interpreted the data, was responsible for the study design, and critically read the manuscript; Mart Saarma initiated the in vivo GFRa1 studies, critically read the manuscript, and provided funding; and Jaan-Olle Andressoo designed and generated glial cell line–derived neurotrophic factor family receptor a1 hypomorphic mice, acquired and interpreted the data, was responsible for the study design, drafted the manuscript, and provided funding.

Conflicts of interest
The authors disclose no conflicts.

Funding
Supported by the Integrative Life Science doctoral program (L.P.); Academy of Finland grant 117044 (M.L.); grants from the Sigrid Juselius Foundation, grant 1186236 from the Academy of Finland, grant R21-AT008265 from the National Institutes of Health, and the Institute of Biotechnology, University of Helsinki (M.S.); by Academy of Finland grant 297727, Sigrid Juselius Foundation, Faculty of Medicine at the University of Helsinki, the Helsinki Institute of Life Science Fellow grant, and by the European Research Council under the European Union's Horizon 2020 research and innovation program, grant agreement 724922 (J.O.A.).